Open access • Proceedings Article • DOI:10.2514/6.2002-374

Aerodynamic Performance of Scale-Model Turbofan Outlet Guide Vanes Designed for Low Noise — Source link

Christopher E. Hughes

Institutions: Glenn Research Center

Published on: 14 Jan 2002

Topics: Bypass ratio, Turbofan, Wind tunnel, Noise and Nacelle

AIAA–2002–0374
Aerodynamic Performance of Scale-Model Turbofan Outlet Guide Vanes Designed for Low Noise

Christopher E. Hughes
NASA Glenn Research Center
Cleveland, OH

40th AIAA Aerospace Sciences Meeting & Exhibit
January 14–17, 2002 / Reno, NV

NASA/TM—2001-211352 AIAA–2002–0374

Aerodynamic Performance of Scale-Model Turbofan Outlet Guide Vanes Designed for Low Noise

Christopher E. Hughes
Glenn Research Center, Cleveland, Ohio

December 2001

The NASA STI Program Office . . . in Profile

Since its founding, NASA has been dedicated to the advancement of aeronautics and space science. The NASA Scientific and Technical Information (STI) Program Office plays a key part in helping NASA maintain this important role.

The NASA STI Program Office is operated by Langley Research Center, the Lead Center for NASA's scientific and technical information. The NASA STI Program Office provides access to the NASA STI Database, the largest collection of aeronautical and space science STI in the world. The Program Office is also NASA's institutional mechanism for disseminating the results of its research and development activities. These results are published by NASA in the NASA STI Report Series, which includes the following report types:

- TECHNICAL PUBLICATION. Reports of completed research or a major significant phase of research that present the results of NASA programs and include extensive data or theoretical analysis. Includes compilations of significant scientific and technical data and information deemed to be of continuing reference value. NASA's counterpart of peer-reviewed formal professional papers but has less stringent limitations on manuscript length and extent of graphic presentations.

- TECHNICAL MEMORANDUM. Scientific and technical findings that are preliminary or of specialized interest, e.g., quick release reports, working papers, and bibliographies that contain minimal annotation. Does not contain extensive analysis.

- CONTRACTOR REPORT. Scientific and technical findings by NASA-sponsored contractors and grantees.

- CONFERENCE PUBLICATION. Collected papers from scientific and technical conferences, symposia, seminars, or other meetings sponsored or cosponsored by NASA.

- SPECIAL PUBLICATION. Scientific, technical, or historical information from NASA programs, projects, and missions, often concerned with subjects having substantial public interest.

- TECHNICAL TRANSLATION. English-language translations of foreign scientific and technical material pertinent to NASA's mission.

Specialized services that complement the STI Program Office's diverse offerings include creating custom thesauri, building customized data bases, organizing and publishing research results . . . even providing videos.

For more information about the NASA STI Program Office, see the following:

- Access the NASA STI Program Home Page at ***http://www.sti.nasa.gov***

- E-mail your question via the Internet to help@sti.nasa.gov

- Fax your question to the NASA Access Help Desk at 301–621–0134

- Telephone the NASA Access Help Desk at 301–621–0390

- Write to:
  NASA Access Help Desk
  NASA Center for AeroSpace Information
  7121 Standard Drive
  Hanover, MD 21076

NASA/TM—2001-211352 AIAA–2002–0374

Aerodynamic Performance of Scale-Model Turbofan Outlet Guide Vanes Designed for Low Noise

Christopher E. Hughes
Glenn Research Center, Cleveland, Ohio

Prepared for the
40th Aerospace Sciences Meeting and Exhibit
sponsored by the American Institute of Aeronautics and Astronautics
Reno, Nevada, January 14–17, 2002

National Aeronautics and
Space Administration

Glenn Research Center

December 2001

Acknowledgments

Acknowledgment is given to General Electric Aircraft Engines for designing the R4 model fan and providing it to NASA as the current technology bypass fan baseline for this test. Also, GEAE designed and fabricated the three model OGV configurations and model nacelle used in this test under NASA Contract NAS3–26617, Task Order 63, and NAS3–98004, Task Order 7.

AIAA–2002–0374

AERODYNAMIC PERFORMANCE OF SCALE-MODEL TURBOFAN OUTLET GUIDE VANES DESIGNED FOR LOW NOISE

Christopher E. Hughes*
National Aeronautics and Space Administration
Glenn Research Center
Cleveland, Ohio

ABSTRACT

The design of effective new technologies to reduce aircraft propulsion noise is dependent on an understanding of the noise sources and noise generation mechanisms in the modern turbofan engine. In order to more fully understand the physics of noise in a turbofan engine, a comprehensive aeroacoustic wind tunnel test program was conducted called the "Source Diagnostic Test." The test was cooperative effort between NASA and General Electric Aircraft Engines, as part of the NASA Advanced Subsonic Technology Noise Reduction Program. A 1/5-scale model simulator representing the bypass stage of a current technology high bypass ratio turbofan engine was used in the test. The test article consisted of the bypass fan and outlet guide vanes in a flight-type nacelle. The fan used was a medium pressure ratio design with 22 individual, wide chord blades. Three outlet guide vane design configurations were investigated, representing a 54-vane radial Baseline configuration, a 26-vane radial, wide chord Low Count configuration and a 26-vane, wide chord Low Noise configuration with 30° of aft sweep. The test was conducted in the NASA Glenn Research Center 9- by 15-Foot Low Speed Wind Tunnel at velocities simulating the takeoff and approach phases of the aircraft flight envelope.

The Source Diagnostic Test had several acoustic and aerodynamic technical objectives: first, establish the performance of a scale model fan selected to represent the current technology turbofan product; second, assess the performance of the fan stage with each of the three distinct outlet guide vane designs; third, determine the effect of the outlet guide vane configuration on the fan baseline performance; and finally, conduct detailed flowfield diagnostic surveys, both acoustic and aerodynamic, to characterize and understand the noise generation mechanisms in a turbofan engine. This paper addresses the fan and stage aerodynamic performance results from the Source Diagnostic Test.

NOMENCLATURE

A	Cross sectional area, in^2
c	Airfoil chord, in
M	Mach number
N	Mechanical fan speed, RPM
N_c	Corrected fan speed, $\frac{N}{\sqrt{\theta}}$, RPM_c
NP_c	Percent of corrected fan design speed, $\frac{N_c}{N_{dp}} \cdot 100$, %
P	Pressure, psia
R	Gas constant, 53.35 ft lbf/lbm°R
T	Temperature, °R
t	Airfoil thickness, in
γ	Specific heat ratio, 1.4
δ	Pressure correction to standard day conditions, $\frac{P_{t,o}}{14.696}$
η	Adiabatic efficiency, $\frac{\left(P_t / P_{t,o}\right)^{\frac{\gamma-1}{\gamma}} - 1}{\left(T_t / T_{t,o}\right) - 1}$
θ	Temperature correction to standard day conditions, $\frac{T_{t,o}}{518.67}$
ω	Weight flow rate, $A_{bm}\sqrt{\frac{\gamma}{R}}\frac{P_{t,bm}}{\sqrt{T_{t,bm}}}\frac{M_{bm}}{\left(1+\frac{\gamma-1}{2}M_{bm}^2\right)^{\frac{\gamma+1}{2(\gamma-1)}}}$, lbm/sec

*Aerospace Engineer, Member AIAA.

ω_c Corrected weight flow rate, $\omega\frac{\sqrt{\theta}}{\delta}$, lbm/sec

Subscripts

ad	Adiabatic efficiency
bm	Bellmouth inlet condition
c	Corrected condition
dp	Design point
f	Fan value
f	Force
m	Mass
max	Maximum value
o	Freestream condition
s	Static condition
st	Stage value
t	Total condition

INTRODUCTION

In recent years, noise from turbofan engines used on commercial aircraft has become a major concern for aircraft owners and airport operators. The increased frequency of takeoffs and landings has produced an increasing number of complaints from local residents. The Federal Aviation Administration in the United States and the International Civil Aviation Organization, the international organization that coordinates environmental noise issues, have responded to these complaints by issuing increasingly more stringent noise regulations and curtailed flight operations for aircraft, forcing aircraft and engine manufacturers to pursue quieter aircraft designs. With the support of Congress, NASA and the U.S. aircraft and engine manufacturing companies have joined to cooperatively investigate high-risk technologies for reducing aircraft noise through program such as the NASA Advanced Subsonic Technology Program.[1,2,3]

As part of the overall NASA program to reduce total aircraft noise, technical efforts were initiated with the major U.S. aircraft engine manufacturers to investigate noise reduction technologies for current technology turbofan engines. NASA established aggressive goals to reduce the noise signature of turbofan engines by the year 2001. Studies were conducted across a wide range of engine operating cycles to identify and quantify the benefit of potential noise reduction concepts. Several noise reduction technology concepts were investigated using scale model wind tunnel testing of turbofan engine simulators, and the noise reduction potential successfully demonstrated in most cases. However, new noise reduction standards and new noise reduction program goals are aggressively pushing the technology. Therefore, in order to more fully understand the noise sources and noise generation mechanisms in a modern turbofan engine, and be able to properly guide further noise reduction technology development, a scale model wind tunnel test of a turbofan simulator was planned called the "Source Diagnostic Test." The test was a cooperative effort between NASA and General Electric Aircraft Engines.

For this test, the bypass stage portion of a medium pressure ratio, high bypass ratio turbofan engine representative of a current technology product was simulated in approximately 1/5 model scale. The test was conducted in the NASA Glenn Research Center 9- by 15-Foot Low Speed Wind Tunnel. Wind tunnel velocities up to Mach number 0.10 were tested, simulating the aircraft initial takeoff and approach phases of operation. The test article consisted of a baseline fan model and several bypass stage outlet guide vane configurations. Only the bypass stage portion, and not the booster core or power stage, of a representative turbofan engine were simulated, eliminating the possibility of contaminating the fan noise field from a core simulation. The test article was powered by the NASA Glenn Ultra High Bypass Drive Rig propulsion simulator.

The Source Diagnostic Test had several technical objectives, both acoustic and aerodynamic. The acoustic performance results from this test are being analyzed and will be presented in a separate document at a later time. The results documenting the LDV and Hot Wire Anemometry aerodynamic flow diagnostic testing obtained in the region around the fan tip and in the fan wake have been published.[4] The aerodynamic test objectives and research results will be addressed in this paper. The aerodynamic objectives of the test were: first, establish the baseline aerodynamic performance level for the scale model fan selected to represent the current technology turbofan product; second, assess the aerodynamic performance levels of the fan stage with each of the three low noise outlet guide vane designs by testing each of them with the fan at the same operating conditions. As part of this objective, the performance losses associated with each of the outlet guide vane configurations are determined; third, determine the effect of the outlet guide vane configuration on the fan baseline performance; and finally, obtain details of the outlet guide vane performance using detailed flowfield surveys on and around the outlet guide vanes. The areas on the outlet guide vanes contributing to the performance losses can then be identified and the losses for each outlet guide vane configuration compared.

TEST APPARATUS

NASA Glenn Research Center 9- by 15-Foot Low Speed Wind Tunnel

The 9- by 15-Foot Low Speed Wind Tunnel (9x15) is an anechoic wind tunnel facility located at the NASA Glenn Research Center in Cleveland, Ohio. The facility is operated as an open loop, continuous flow wind tunnel at atmospheric pressure conditions. The test section is located in the flow return portion of the NASA Glenn 8- by 6-Foot Supersonic Wind Tunnel flow circuit. The two wind tunnels share a common drive system to generate airflow in the test section. Figure 1 shows the 8- by 6-Foot Supersonic Wind Tunnel/9- by 15-Foot Low Speed Wind Tunnel Complex. The wind tunnel is capable of producing velocities in the test section from Mach number 0.0 to 0.23.[5] Static testing can also be conducted in the test section. The facility produces very low freestream turbulence and distortion levels, making it ideal for acoustic testing of propulsion systems.[6] The test section surfaces are covered with boxes filled with an acoustic treatment material that is capable of absorbing sound reflections down to 250 Hz.[7]

Turbofan Propulsion Simulator

A propulsion simulator called the NASA Glenn Ultra High Bypass (UHB) Drive Rig was used to power the model fan test article. Details about the UHB Drive Rig can be obtained from a report documenting the General Electric Aircraft Engines (GEAE) Universal Propulsion Simulator,[8] which is very similar to the NASA Glenn UHB Drive Rig simulator. Figure 2 is a schematic diagram of the UHB Drive Rig. A four-stage air turbine generates the power that is supplied to the fan model through a common shaft connection. The air turbine is driven by high pressure (up to 350 psi), high temperature (up to 550 °F) air that is supplied to it from tubes running through a support strut that mounts the UHB Drive Rig in the wind tunnel test section. The UHB Drive Rig can generate up to 5,000 shaft horsepower at 17,000 RPM. Figure 3 is a schematic diagram of the UHB Drive Rig installation in the wind tunnel test section.

Fan Module

The test article, or fan module, was a 1/5-scale model representation of the bypass stage of a current generation high bypass turbofan aircraft engine. The fan module was designed and built by GEAE with partial funding from NASA. Only the bypass section of the engine was simulated, not the power core section, to remove any possible contamination of the fan and outlet guide vane noise field from the core simulation noise. The fan module consisted of the fan, the outlet guide vanes (OGVs) and a flight-type nacelle, which included a flight-type inlet, a cowl and a fixed-area, flight-type nozzle. In order to concentrate on the fan and OGV noise, the OGVs were used to provide support for the nacelle in the model, thereby eliminating the need for the pylon, struts and internal bifurcation normally present in a turbofan engine. Figure 4 is a schematic diagram of the fan module in the flight configuration, used for acoustic testing, installed on the UHB Drive Rig. Figure 5 shows the fan module in the flight configuration and the UHB Drive Rig installed in the 9x15.

The fan used for this test was 22 inch diameter and had 22 individual, wide chord blades. Figure 6 shows several views of one of the fan blades. It represented a medium pressure ratio bypass fan design, with a stage design point pressure ratio of 1.47 at a model corrected speed of 12,657 RPMc, which corresponds to a design point fan tip speed of 1,215 feet per second. Table 1 provides a summary of the design parameters for the fan. The fan was a scale model designed and previously tested by GEAE, who designated the fan as “R4.” The fan was originally designed to operate in conjunction with a powered core simulator. As a result, the performance level at its design point could not be achieved in this test since this installation did not include a core simulation. However, since this fan was meant to be representative of current technology, the performance compromise was deemed to be acceptable for this test. The fan was tested with a .020” blade tip clearance at the design point (100% corrected fan speed, or 12,657 RPMc). This clearance was selected as representative of a turbofan engine with many takeoff and landing cycles. In addition, this tip clearance minimized the chance of a fan rub event during testing, thus insuring a clean and uniform flowpath contour at the fan tip that is important for producing uncontaminated acoustic results.

As part of the fan module design, there were three distinct OGV designs, representing an acoustic baseline and two additional configurations designed to reduce the level of specific noise sources in the fan module. In order to maintain the aerodynamic loading for each OGV configuration, the solidity between the three designs was held nearly constant. In addition, the flowpath geometry was designed to achieve as close to the same flow velocity as possible between the three designs. Table 2 is a summary of the design parameters for the three OGV configurations. The Baseline OGV configuration, representative of a current technology design for this pressure ratio fan, had 54 narrow chord, high aspect ratio vanes. The blade/vane ratio allowed the first blade passing frequency (BPF) tone of the fan to be cut-off. Figure 7a is a schematic representation of the Baseline OGVs in the fan module, and Figure 7b shows the fan and Baseline OGVs with the nacelle

removed mounted on the UHB Drive Rig in the wind tunnel. The second OGV design, called the Low Count OGVs, had 26 wide chord, low aspect ratio vanes. Figure 8 shows a schematic diagram and photos of the Low Count OGVs. While the blade/vane ratio allowed the first BPF to be cut-on, the acoustic objective was to reduce the broadband noise signature by reducing the total number of vanes. The third OGV design, called the Low Noise OGVs, had 26 wide chord, low aspect ratio vanes as well, but also incorporated 30° of aft sweep into the vane geometry.[9,10] Figure 9 shows a schematic diagram and photos of the Low Noise OGVs. The vane was rotated backwards from a point at the hub leading edge, which represents a displacement aft of approximately one chord length at the tip of the vanes. The tone noise is reduced because there is an increase in the axial spacing between the fan and the swept OGV that weakens the fan wake strength and therefore the acoustic strength of the fan wake and OGV interaction. In addition, the tone noise is reduced by introducing a phase variation along the span of the vane, from the hub to the tip, when the fan wake strikes the swept vane leading edge. In other words, a given radial line in the fan wake moving downstream does not strike the OGV leading edge all at once, but rather intersects the swept vane leading edge in a scissor-like fashion.

While the two reduced vane count OGVs were designed to reduce noise through changes in the vane geometry, there were also aerodynamic requirements imposed on the vane designs as a result of the acoustic requirements. The noise produced by the OGVs is in part a function of the steady and unsteady aerodynamic loading on the vanes and the local flowfield velocity distributions. Therefore, in order to make a noise comparison between the three OGV configurations as equal as possible, the total aerodynamic loading for each OGV configuration was kept as equal as possible. Any differences in the noise between OGV configurations could then be attributed to variations in the number of vanes and in the vane physical geometry, and not to differences in the aerodynamic performance characteristics of the OGVs. The aerodynamic loading on the OGVs is partly a function of the total airfoil surface area, so the loading between the three designs was kept as close as possible by keeping the vane solidity nearly constant. The solidity is the ratio of the vane airfoil chord length to the gap between vanes at a given spanwise location on the vane. At a constant solidity, the vane airfoil chord grows longer and the gap between vanes gets larger as the number of vanes is reduced, keeping the total airfoil area the same for each configuration. With almost half the number of vanes, the chord length of the Low Count and Low Noise OGVs was nearly twice the length of the vane chord length on the Baseline OGVs. Some compromise in the acoustic requirements for the OGV designs was required in order to minimize the aerodynamic performance losses of the larger vanes, however, such as keeping the velocity distributions on the vanes to acceptable levels to prevent large pressure drag losses. For the Low Noise OGV configuration, the velocity profiles on the vane flow surfaces are higher compared with the other two OGV designs, especially at the outer region on the vane near the tip, in order to carry the same total aerodynamic loading.

To establish the fan and OGV performance, the fan module installation included a uniform-inflow bellmouth inlet and either the fixed-area flight-type nozzle or a Variable area Fan Exit Nozzle (VFEN). The fixed area nozzle was used to obtain the fan performance on a representative operating line for a turbofan engine installation, at sea level conditions. Figure 10a shows a diagram of the bellmouth inlet and fixed area nozzle installed on the UHB Drive Rig during fan performance testing, and Figure 10b shows the fixed nozzle operating line configuration in the wind tunnel. The VFEN was used to obtain fan and stage performance across a range of fan speed operating conditions and simulated aircraft flight conditions. It consisted of a series of trapezoidal-shaped plates, each with a central radial pivot, arranged circumferentially in an annular duct. The plates moved in pairs in opposing directions to one another, like double doors. The fan operating point was changed by varying the exit area, and therefore the back pressure on the fan, while at a constant fan speed. Changing the fan back pressure simulates a change in the aircraft flight speed and altitude. Figure 11a is a diagram of the bellmouth inlet and VFEN installed with the fan module during performance testing. Figure 11b shows this configuration installed in the wind tunnel, and Figure 11c shows a close-up view of the VFEN.

Instrumentation

Freestream conditions in the wind tunnel were determined using a ceiling mounted pitot-static rake with thermocouples located near the entrance to the test section. Fan inlet conditions were determined using a floor mounted, cruciform-shaped rake located near the fan centerline and upstream of the bellmouth inlet. Total pressure and total temperature conditions directly upstream of the fan were measured with this rake. Figure 12 shows the fan module and the cruciform rake installed in the test section. Within the fan module, the fan weight flow was determined from static pressure measurements obtained within the bellmouth inlet and a flow correlation function relating the average of the bellmouth static pressures and the fan weight flow.

Fan and stage performance were determined using fixed total pressure/total temperature rakes mounted behind the fan and OGVs. Fan performance was obtained using three rakes and stage performance was

obtained with seven rakes. Each rake consisted of seven measurement sensors, and each sensor contained a total pressure probe and a total temperature probe co-located within an aspirated stagnation tube. The sensors on each rake were located radially in such a way as to provide flow conditions at the center of equal areas. In addition, surface mounted static pressures were located at several axial locations in the fan module for calculating internal velocities.

Figures 13a and 13b are diagrams of the instrumentation locations in the fan module for performance measurements with the model in the fan mapping and in the fixed operating line performance testing configurations, respectively. During the fixed operating line testing with the fixed area nozzle installed, only fan performance could be measured, since the stage performance rakes could only be installed in the model with the VFEN in place.

TEST PROCEDURE

The fan and OGV, or stage, aerodynamic performance was obtained for the fan and in combination with each OGV configuration. A Mach number of 0.05 was set in the test section during testing in order to provide uniform temperature and pressure distributions into the fan, and also to prevent the fan from creating and ingesting vortices from the test section surfaces. To eliminate the day-to-day variations in pressure and temperature that affect the performance calculations, the fan and stage performance parameters were corrected to standard day pressure and temperature conditions, where required. To insure that data was acquired at steady state conditions, a 30 second settling time interval was maintained after each new fan operating condition was reached. In addition, pressure and temperature information from the data system was time averaged over a 10 second sampling.

Fan and Stage Mapping

Fan and stage performance mapping was conducted with the bellmouth inlet and the VFEN installed on the fan module. A performance map is a plot of the measured fan or stage performance parameter (total pressure ratio, total temperature ratio, or adiabatic efficiency) as a function of the corrected fan weight flow for a series of constant fan speed lines along which the fan weight flow is varied from minimum (toward a fan stall condition) to maximum (toward the aircraft high velocity/high altitude cruise condition) with the VFEN. The fan stall condition was avoided in order to minimize the risk of potentially damaging the fan blades if a rapid hard stall was encountered that produced a fan rub, even though the fan rubstrip was designed for fan tip incursions. With this fan design, an approaching stall condition was usually indicated by an increase in the fan blade stress. Therefore, the minimum fan weight flow was achieved when the fan blade stress measured with blade mounted strain gauges reached a predetermined limit. This limit varied with fan speed. The maximum weight flow was achieved at the maximum nozzle area with the VFEN fully open. Corrected fan speeds from 50% to 100% of corrected fan design speed were set, corresponding to corrected fan speeds from 6,328 to 12,657 RPM_c. For the stage adiabatic efficiency, the assumption was made that there is no loss in total temperature loss across the OGVs and therefore the total temperature data from the fan performance rakes were used in the calculations. In this way, variations between temperature measurements made with the fan rakes compared with the stage rakes that would introduce larger errors in the calculation of stage adiabatic efficiency could be eliminated. Overall values for the fan and stage performance were obtained by averaging the seven radial profile values for each performance parameter.

In order to more directly compare the stage performance between OGV configurations, a stage performance loss coefficient for total pressure was defined. This loss coefficient was used as a measure of the performance drop across the OGVs, in percent, and was expressed as,

$$Loss\ Coefficient = \frac{\left(P_{t,f} - P_{t,st}\right)}{P_{t,f}} \cdot 100 ,$$

Using the stage total pressure loss coefficient, the maximum stage performance, or minimum total pressure loss coefficient, on the stage performance map was determined.

Fixed Nozzle Operating Line

Fan performance on the operating line represented by the fixed area nozzle near sea level conditions was obtained using the bellmouth inlet and fixed area, flight-type, nozzle. Corrected fan design speeds from 40 to 100.7%, corresponding to 5,063 to 12,746 RPM_c, were set. This fan speed range represented engine power settings from ground idle to full power takeoff. With the fixed area nozzle installed, only the fan performance was obtained since the stage performance rakes could only be installed with the VFEN testing configuration. However, once the fan weight flow and fan operating parameters were established for the fixed nozzle operating line, the corresponding stage performance was obtained with the VFEN installed by adjusting the nozzle exit area to match the fixed nozzle fan performance at the corresponding fan operating conditions.

RESULTS AND DISCUSSION

For the results presented in this section, the accuracy of the performance calculations is based on empirical observation and repeat data points. The accuracy of the data acquisition systems used during testing were ± 0.002 psia for pressure and ± 0.25 °F for temperature. However, the data systems were configured to provide time-averaged measurements at a high sample rate. For temperature and pressure, the data values are based on an average of ten, one-second averages, with each one-second average based on the average of 20,000 samples. Therefore, the accuracy of the discrete performance points is higher than the results based on discrete data samples. For pressure ratio, the accuracy of calculation is ±0.0003; for temperature ratio, the accuracy of the results is ±0.001; and for adiabatic efficiency, the accuracy of the results is ±0.003.

Fan Performance Maps

The fan total pressure ratio, total temperature ratio and adiabatic efficiency performance maps are presented in Figures 14a through 14c. The Low Noise OGV configuration was installed in the fan module during this testing. Although the fan performance with all three OGV configurations was obtained, the variation in fan performance with OGV configuration was insignificant. Therefore, this is the only OGV configuration for which fan performance results will be presented. Later in this report, results supporting this observation will be presented in the discussion of the fan performance on the fixed nozzle operating line. The fan results with this OGV configuration were selected for presentation because they are the most complete in terms of fan operating range. For reference, the fixed nozzle operating line results obtained during testing at sea level conditions are shown as the solid line that crosses the fan speed lines. The fan performance at the three operating conditions used for engine noise certification known as the acoustic rating points, representative of the aircraft flight operating points at approach, cutback, and takeoff (61.7, 87.5, and 100% corrected fan speed), for this fan design are shown as solid symbols on the fixed nozzle operating line in all the figures.

Figure 14a shows the total pressure ratio fan map and Figure 14b shows the total temperature ratio fan map. In both figures, the minimum fan weight flow operating point on each fan speed line appears close to the fixed nozzle operating line, which would seem to indicate that the fan stall line is close to the fixed nozzle operating line. However, as discussed earlier, the minimum fan weight flow condition on each fan speed line represents a fan blade stress limit to prevent fan stall. Although not shown, the fan stall line would be located further to the left in both figures, while the high altitude/cruise line would be to the right of the fixed nozzle operating line. Since the stall line was not approached, the characteristic flattening and rollover in the performance curves at lower fan weight flow conditions and at higher fan speeds do not appear.

The adiabatic efficiency fan map is shown in Figure 14c. The fixed nozzle operating line results are again shown as the solid line that intersects all the fan speed lines. In the figure, the fixed nozzle operating line does not appear very smooth over the fan weight flow operating range. This is a result of using the VFEN to set the fixed nozzle operating conditions on each speed line, because the VFEN area could not be set precisely enough to repeat exactly the fixed nozzle fan operating conditions. At the lower fan speed lines, the fan performance never reaches a rollover, or peak, point but continues to increase as the fan weight flow increases. As the fan speed increases, the results indicate a slight wiggle in the adiabatic efficiency at the higher weight flow conditions for speeds at 87.5% corrected fan speed and lower. The reason for this phenomena is not clear, but may be an indication of a flow transition or flow instability on the fan blade at those fan speeds and aerodynamic loading conditions. The adiabatic efficiency begins to exhibit a peak in the performance level beginning at the 87.5% corrected fan speed line. The performance peaks at the highest fan speed lines are fairly sharp, indicating the sensitivity of the fan blade to incidence angle at the higher weight flow conditions. The fan adiabatic efficiency reaches the highest level of 0.926 or 92.6%, at 101.4 lbm/sec weight flow on the 100% corrected fan speed line, near the fan weight flow design point. For this type of high bypass fan design, the peak performance is considered to be on the low side. However, as discussed earlier, this was a pre-existing fan, designed to be used with a core simulator, and therefore the level of fan performance was deemed to be acceptable. The fan performance results are being shown as documentation and as a reference for the stage performance to be presented in later sections, and not being used to rate the fan design. On the fixed nozzle operating line at sea level conditions, the results show that the adiabatic efficiency is down significantly from the peak levels at all fan speed lines, from 1.4% at higher fan speeds to 3.4% at lower fan speeds, indicating that the fan operates fairly far off from the optimum fan performance.

The fan total pressure ratio, total temperature ratio and adiabatic efficiency performance results on the fixed nozzle operating line for the three acoustic rating point speeds (approach, cutback and takeoff) and the fan design point are summarized in Table 3.

Stage Performance Maps

In Figures 15 through 17, the stage total pressure ratio and stage adiabatic efficiency maps for all three OGV configurations tested are presented. As discussed earlier, only the stage total pressure ratio and adiabatic efficiency are shown as a function of the corrected fan weight flow, since the fan total temperature ratio results were used in the calculation of the stage adiabatic efficiency.

Baseline OGVs: A summary of the Baseline OGV performance at the three acoustic rating speeds and the fan design point are given in Table 4.

The stage total pressure ratio results are shown in Figure 15a. The trend in the results is the same as that observed for the fan, especially the roll-off characteristics at the higher fan speeds. This indicates that the fan and OGV performance is being driven by the fan operating characteristics and not by the OGV flow characteristics, so the OGV flow is not choked. The test results do not go very far to the left of the fixed nozzle operating line, toward lower fan weight flows and fan stall. The reason is that at this point in the test the fan strain gages monitoring blade stress had stopped working, and so the fan operating conditions were conservatively set to higher fan weight flows to avoid unintentionally entering a stall condition.

Figure 15b shows the stage adiabatic efficiency for the Baseline OGVs. Here, the data trends are significantly different compared to the fan adiabatic efficiency results shown earlier. The results show a peaking and then a roll off in the performance curves at every fan speed line. This is a result of the higher losses on the OGVs produced by the sensitivity of the OGV performance to the inflow incidence angle, and possibly due to higher total pressure losses inboard on the vanes where the vane-to-vane passage is the narrowest, or the tip where the flow velocity is the highest. The highest adiabatic efficiency was seen at on the 100% fan speed line. At the fan design point, the results indicate the loss in adiabatic efficiency across the Baseline OGVs is on the order of 3%. For a bypass stage design, this loss number is higher than expected, but acceptable when considering the design constraint of using a pre-existing fan that has not been optimized for this operational application.

Low Count OGVs: A summary of the Low Count OGV performance at the three acoustic rating speeds and the fan design point are given in Table 5.

The stage performance for the Low Count OGVs is presented in Figures 16a and 16b. Figure 16a shows the stage total pressure ratio fan map, and Figure 16b shows the stage adiabatic efficiency. The trends in the performance results are very similar to the Baseline OGV results. These performance levels shown are very close to those for the Baseline OGVs.

The Low Count OGV stage adiabatic efficiency is shown in Figure 16b. The Low Count OGV adiabatic efficiency performance is also close to the results shown for the Baseline OGVs, especially at the peak performance points. At conditions away from the peak levels, the adiabatic efficiency drops slightly below the performance of the Baseline OGVs, especially at the higher fan speeds possibly due to an increase in losses associated with the longer vane chord lengths. However, the results indicate that the Low Count OGV design was successful in matching the aerodynamic loading of the Baseline OGVs at the design point.

Low Noise OGVs: A summary of the Low Noise OGV performance at the three acoustic rating speeds and the fan design point are given in Table 6.

The Low Noise OGV stage performance results are shown in Figures 17a and 17b. The Low Noise OGV total pressure ratio is shown in Figure 17a. Again, the trends in the results are similar to the Baseline and Low Count OGV total pressure ratio results. The results show that the total pressure ratio does not reach as high a value as the other two OGV configurations along a speed line. Also, the fan weight flow at those fan speeds is also slightly lower compared with the Baseline and Low Count OGVs.

The Low Noise OGV adiabatic efficiency results are shown in Figure 17b. The adiabatic efficiencies are lower compared to the other OGVs at all the fan speed lines, but especially at the lower fan speed conditions. The trend in the data at the 100% fan speed line also show the performance to have a sharper peak at the maximum level compared with the other OGVs, indicating more sensitivity of the performance flow incidence angle at off design operating conditions. The results show that the performance is lower than the other two OGV configurations, indicating that there is an increase in the losses across the Low Noise vanes. This may be associated with the higher flow velocities on the Low Noise vanes, since these OGVs were designed to operate with a higher velocity distribution on the airfoils compared with the other two OGV configurations.

Stage Performance Losses

In Figures 18 through 20, the performance loss coefficient results for the stage total pressure and stage adiabatic efficiency for the three OGV configurations are presented.

Baseline OGVs: A summary of the Baseline OGV performance losses at the three acoustic rating speeds and the fan design point are given in Table 7.

Figures 18a and 18b show the stage performance loss results for the Baseline OGVs. The stage total pressure loss coefficient results are shown in Figure 18a. The results show that the Baseline OGVs

have a reasonable total pressure loss at all fan speed lines across the range of fan weight flows tested. The distribution of the loss coefficients on each fan speed line also show a favorable trend, with a fairly wide bucket or area where the loss coefficients remain near the minimum value. These results indicate that the Baseline OGVs are somewhat insensitive to flow incidence angle, so reasonable stage performance levels are achieved at off design conditions, such as the fixed area nozzle operating line. The results also show that the loss coefficients are the lowest at the lowest fan speed line and increase with increasing fan speed and weight flow. This trend is expected, since the pressure losses across the OGVs increase at the higher flow rates and, therefore, higher flow velocities. However, the total pressure losses are still reasonable, near 1.5%, even at 100% corrected fan speed and the higher corrected fan weight flow rates.

Figure 18b shows the stage adiabatic efficiency loss results for the Baseline OGVs. A performance assessment of the OGV design can readily be seen in this type of figure. The results show that the stage adiabatic efficiency losses are somewhat larger than what would be expected for the bypass stage performance. However, as was discussed earlier, the performance levels are reasonable for an unoptimized fan/OGV design configuration, particularly at the minimum loss point. Interestingly, the results also show that the optimum stage adiabatic efficiency performance/minimum loss points lie in a fairly flat line across the fan speed line range. The adiabatic efficiency losses increase rapidly at conditions away from the minimum loss point. For the Baseline OGVs, the fixed nozzle operating line is close to the minimum loss level at all fan speeds, indicating that the Baseline OGVs were well designed for minimum losses and maximum performance at those operating conditions. The design point results are interesting and may indicate that at the higher fan weight flow conditions for these OGVs, the performance losses are higher, possibly due to local flow conditions in the narrow passages at the hub of the vanes.

Low Count OGVs: A summary of the Low Count OGV performance losses at the three acoustic rating speeds and the fan design point are given in Table 8.

The Low Count OGVs stage performance loss coefficients are shown in Figures 19a and 19b. Figure 19a shows the results for the Low Count OGVs total pressure loss coefficient. The data follows the same trend as the total pressure loss coefficient results for the Baseline OGVs, with the lowest loss coefficient observed at the low fan speeds and increasing at the higher fan speeds. However, the minimum loss bucket has a slightly narrower range for these OGVs compared with the Baseline OGVs, meaning the Low Count OGVs performance is more sensitive and less tolerant to changes in the flowfield as the fan weight flow operating conditions change. The results show that the level of the total pressure loss coefficient is still reasonable, with the value of the loss coefficient at the lowest point only slightly higher for the Low Count OGVs compared to the Baseline OGVs. Also, the design for the Low Count OGVs was successful by achieving the minimum loss coefficient at the fan design point weight flow. But because of the increase in performance sensitivity at off design conditions, the Low Count OGV fixed nozzle operating line performance is further away from the minimum loss coefficient compared with the Baseline OGVs.

Figure 19b shows the Low Count OGV stage adiabatic efficiency loss results. The data trends appear similar to those observed for the Baseline OGVs, with the minimum loss points that are fairly constant with increasing fan weight flow and sharply increasing losses away from the minimum loss point. As with the total pressure loss coefficient results, the adiabatic efficiency loss curves along each fan speed line exhibit narrower loss buckets, with the losses increasing more quickly away from the minimum loss point, compared with the Baseline OGVs. At the higher fan speed conditions, the losses are slightly higher than the Baseline OGVs over the entire range. This is an indication of higher losses associated with the Low Count OGV vanes, possibly as a result of the longer vane chord and higher drag at higher weight flows and velocities. The value for the minimum loss point for each fan speed line is very similar to the Baseline OGVs, except at the higher fan speed lines, which show a slightly higher loss at the minimum point compared with the Baseline OGVs. For the fixed nozzle operating line, the adiabatic efficiency loss is larger as the fan speed and fan weight flow increase compared with the Baseline OGVs, indicating that the Low Count OGV is not at the optimum performance design condition. At the fan design weight flow point, the adiabatic efficiency loss was nearly the same as the Baseline OGV adiabatic efficiency loss. The stage performance levels for the Low Count OGVs were considered relatively good compared with the Baseline OGV performance, especially at fan speeds below 100%. The performance losses were higher than expected at the higher fan speeds, but still reasonable for this wide chord, non-optimized vane design.

Low Noise OGVs: A summary of the Low Noise OGV performance losses at the three acoustic rating speeds and the fan design point are given in Table 9.

The stage performance loss results for the Low Noise OGVs are shown in Figures 20a and 20b. The stage total pressure loss coefficient results for the Low Noise OGVs are shown in Figure 20a. Here, the data trends show that the total pressure loss coefficient minimum loss buckets narrow even further for each fan

speed line compared with the other two OGV configurations. These results indicate that the Low Noise OGVs performance losses are even more sensitive to off design conditions than the Low Count or Baseline OGVs, with larger losses experienced compared to the other OGVs as the flow conditions move away from the Low Noise OGV design optimum. In addition, the loss coefficients are slightly higher at the minimum loss point compared with the other OGVs, indicating an additional loss mechanism for these OGVs compared with the other two configurations. As a result, the fixed nozzle operating line total pressure loss coefficients are larger than the other two OGVs. At the corrected fan design weight flow point at 100% corrected fan speed, the results show the minimum loss point was reached.

The Low Noise stage adiabatic efficiency loss results are shown in Figure 20b. The data show the loss curves to be narrower over the fan speed line and have smaller minimum loss buckets compared to the Low Count OGVs and the Baseline OGVs. The same trend in the data shown for the other two OGVs configurations can be seen in these results, with the minimum loss value nearly a constant across the fan speed lines at 87.5% corrected fan speed and below, and the minimum loss value increasing at speeds above 87.5% corrected fan speed. The minimum loss points on the curves, however, have higher values for the Low Noise OGVs, meaning there are higher losses across the vanes at all operating conditions compared with the other two OGVs. These higher losses may be a result of the higher velocity distributions on the outer portion of the vanes that were part of the Low Noise OGV design. On the 100% corrected fan speed line, the minimum loss values increase much more than what was seen for the Low Count OGVs, indicating the higher losses on the Low Noise OGVs at this speed. The adiabatic efficiency loss curves are also narrower compared with the other two OGV configurations, and so the fixed nozzle operating line is further from the minimum loss point on the curve; therefore, the performance is lower and the losses larger compared with the other OGVs. At the fan design weight flow point, the adiabatic efficiency loss coefficient was very near the minimum value for the 100% corrected fan speed line, indicating that the OGVs did minimize the losses at that speed line for the fan design point. But overall, the stage performance for the Low Noise OGVs is lower than what is considered reasonable for conventional OGVs in a turbofan engine. However, because of the design constraints placed on the OGV design by the acoustic requirements, the model installation requirements, and the aerodynamic requirements from a fan design that was not optimized to operate with the swept OGV design, the stage performance results are considered acceptable and reasonable for this test in order to validate the acoustic performance differences.

Fixed Nozzle Operating Line Performance

Although the fixed nozzle operating line performance results were shown in conjunction with the performance map results in the previous sections, the fixed nozzle performance results are being presented separately to show details of the fixed nozzle operating line performance at sea level conditions and highlight the differences in the fan performance and operating conditions with different OGV configurations, and also to allow a direct comparison the differences in performance between OGV configurations.

Fan Performance: The fan performance results with the fixed area nozzle are shown in Figures 21a through 21d. The results in these figures also show a comparison of the fan performance with the three OGV configurations. The results show that the fan performance was insensitive to the OGV configuration installed during testing. Figure 21a shows the corrected fan weight flow as a function of corrected fan speed for the three OGV configurations. As can be seen, the corrected fan weight flow was nearly the same for all three OGV configurations. The Low Noise OGVs show a slightly lower fan weight flow compared to the Baseline and Low Count OGVs. At 100% corrected fan speed, this difference between was only 0.25 lbm/sec, and is considered to be within the error band of the calculation. Figures 21b and 21c compare the fan total pressure ratio and fan total temperature ratio, respectively, for all three OGV configurations. The results show that the fan performance was nearly identical for all three OGVs. Figure 21d shows the fan adiabatic efficiency on the fixed nozzle operating line for the three OGV configurations. The adiabatic efficiency results are more sensitive to differences in performance and show the differences between OGV configurations more easily. The results confirm that the fan performance was nearly the same for all three OGV configurations. Small differences in the adiabatic efficiency, especially toward the lower fan weight flow conditions, can be attributed to accuracy errors in the results, since the values of pressure ratio and temperature ratio are very low at these conditions.

Stage Performance: The stage performance results for the three OGV configurations on the fixed nozzle operating line conditions are shown for the stage total pressure ratio and stage adiabatic efficiency in Figures 22a and 22b, respectively. As expected, the results indicate the Baseline OGVs have the highest total pressure ratio and the highest adiabatic efficiency compared with the Low Count and the Low Noise OGVs. The differences in performance between the Baseline and the Low Count OGV configurations are

very small across the fan weight flow range. The differences in the stage adiabatic efficiency is less than 0.25% until the corrected fan weight flow reaches 90 lbm/sec, or about 95% corrected fan speed when the differences get slightly larger. At 100% corrected fan speed, the difference in stage adiabatic efficiency is 0.4%. The Low Noise OGVs results show larger differences across the fan weight flow range, but still within 0.25% until the corrected fan weight flow reaches 66 lbm/sec, or about 70% corrected fan speed. At 100% corrected fan speed, the difference in stage adiabatic efficiency between the Low Noise OGVs and the Baseline OGVs is 1.1%.

Stage Losses: In Figures 23a and 23b, the stage loss coefficients on the fixed nozzle operating line as a function of the corrected fan weight flow is presented for the three OGV configurations. Figure 23a shows the stage total pressure loss coefficient results and Figure 23b shows the stage adiabatic efficiency loss results. The Baseline OGVs exhibited the best performance across the entire fan weight flow operating range. However, the Low Count OGV performance was equal to the Baseline OGV at the corrected fan weight flow conditions below 70 lbm/sec, or about 74% corrected fan speed. As the flow velocities increase with an increase in the fan weight flow, the higher losses on the Low Count OGVs caused a performance drop, especially at the higher fan speeds and fan weight flow conditions. As stated earlier, this performance drop may be result of an increase in losses associated with the longer vane chord lengths, especially at operating conditions away from the design conditions. The Low Noise OGV performance was consistently lower than the performance of the other two OGVs across the fan weight flow range. As with the Low Count OGVs, the longer chord length on the Low Noise OGVs may have increased the losses on the vanes compared with the Baseline OGVs. In addition, the higher velocity distributions associated with the Low Noise OGV design attributed to the vane losses. For the stage total pressure loss coefficient results, the largest difference measured between the Baseline and Low Count OGVs was 0.18%, and between the Baseline and the Low Noise OGVs was 0.41% at 100% corrected fan speed. For the stage adiabatic efficiency loss, the largest difference measured between the Baseline and the Low Count OGVs was 0.49%, and between the Baseline and the Low Noise OGVs was 1.15% at 100% corrected fan speed.

SUMMARY AND CONCLUSIONS

The aerodynamic performance testing of a 1/5-scale model of the bypass stage portion of a modern turbofan engine was conducted in the NASA Glenn 9- by 15-Foot Low Speed Wind Tunnel. The wind tunnel model configuration consisted of a 22 bladed, 22 inch diameter fan, three outlet guide vane (OGV) configurations designed to reduce noise, and a nacelle. Testing was conducted at seal level conditions and at speeds simulating the takeoff and approach phases of the aircraft flight envelope. A range of fan speeds and fan weight flows was investigated using fixed and variable area exit nozzles to simulate the fan and aircraft flight operating conditions.

Performance results are expressed in terms of the total pressure ratio, total temperature ratio and adiabatic efficiency for the fan, and total pressure ratio and adiabatic efficiency for the stage, which includes the OGVs, at each operating point. In addition, the stage performance results are expressed in terms of a total pressure loss coefficient and adiabatic efficiency loss, which provide a direct assessment of the performance losses across the OGVs.

The fan performance results show that the following:

1. The fan model used in the test was a reasonable scale model simulation of the fan from a current generation turbofan engine comparing the model performance to what is expected from the full-scale fan performance. The performance level achieved during this test was lower than expected, however, possibly because the fan was a pre-existing model and was designed for use in a wind tunnel model with a powered core simulator, which was not used during this test. At the fan design point at 100% corrected fan speed at corrected fan weight flow of 100.5 lbm/sec, the fan achieved a pressure ratio of 1.488, at total temperature ratio of 1.130, and an adiabatic efficiency of 0.924, with the Low Noise OGVs installed. On the operating line, representing the fixed nozzle area at sea level and simulated takeoff/approach flight speed conditions, the highest fan performance was measured at the 100% corrected fan speed, representing full takeoff power, with a total pressure ratio of 1.508, a total temperature ratio of 1.137 and an adiabatic efficiency of 0.912 at a corrected fan weight flow of 96.7 lbm/sec.
2. The fan performance was fairly insensitive to the OGV configuration installed during testing, since the fan adiabatic efficiency performance did not vary significantly between OGV configurations.

The stage performance results indicate the following:

1. The level of performance for all three OGV configurations was slightly lower than expected; however, since the fan model used was a pre-existing, non-optimized design, the

performance for the OGVs was considered acceptable in this application for this test in order to verify the potential of the reduced noise OGV design.

2. The Baseline OGVs had the highest performance of the three OGV configurations. The Low Count and Low Noise OGVs showed performance below the Baseline OGVs, but the difference was considered acceptable since: 1) the OGVs were designed to reduce noise and were not optimized for maximum performance; and 2) the OGV designs were constrained by the existing fan design and flowpath geometries. The performance for all three OGVs was close near the peak adiabatic efficiency point on each fan speed line. Differences in performance were more pronounced away from the peak efficiency. On the fixed nozzle operating line, the Low Count OGV performance was close to the Baseline OGV performance below 87.5% corrected fan speed, and dropped below the Baseline OGVs at higher fan speeds. The Low Noise OGV performance was lower than the Baseline or the Low Count OGVs at all fan speeds.
3. The highest stage performance for all three OGV configurations was obtained near the fan design point at 100% corrected fan speed and 100.5 lbm/sec corrected fan weight flow. The stage performance at the fan design point was: for the Baseline OGVs, an adiabatic efficiency of 0.890 at a total pressure ratio of 1.470; for the Low Count OGVs, an adiabatic efficiency of 0.891 at a total pressure ratio of 1.470; and for the Low Noise OGVs, an adiabatic efficiency of 0.887 at a total pressure ratio of 1.466.

For the stage performance loss results, several trends can be seen:

1. The Baseline OGVs have the highest performance with the lowest total pressure ratio and adiabatic efficiency losses at all fan speeds, followed by the Low Count OGVs and finally the Low Noise OGVs.
2. A minimum loss bucket exists on each fan speed line for all three OGVs. The losses increase dramatically on either side of the bucket as the inflow incidence angle on the vanes moves away from the design angle for optimum performance.
3. The minimum loss point in the adiabatic efficiency loss curves at each fan speed line for each of the OGVs is nearly constant, except at fan speeds above 87.5% corrected fan speed for the Low Count and the Low Noise OGVs. As the fan speed and weight flow increase, the Low Count and Low Noise OGV results show slightly higher losses since the minimum loss point increases at these conditions for those OGV configurations compared with the Baseline OGVs. The losses may be associated with the longer airfoil chord lengths or, in the case of the Low Noise OGVs, the higher flow velocities on the vanes as part of that vane design.
4. For the Baseline OGVs, the minimum adiabatic efficiency losses coincide closely with the fixed nozzle operating line at all fan speeds, indicating that the Baseline OGVs were well designed for that operating line. The performance loss, however, for the Low Count and Low Noise OGVs is higher on the fixed nozzle operating line, indicating a high sensitivity of the OGV performance to off design inflow incidence angles.

In conclusion, the scale model test results show that an outlet guide vane configuration for the bypass portion of a turbofan engine can be designed to reduce the noise produced by the bypass stage, while at the same time achieve acceptable aerodynamic performance, compared with a conventional bypass outlet guide vane design.

REFERENCES

1. Groeneweg, J.F., "Fan Noise Research at NASA," NASA TM–106512, 1994.
2. Envia, E., "Fan Noise Reduction: An Overview," NASA/TM—2001-210699, AIAA–2001–0661, 2001.
3. Bridges, J., Envia, E., and Huff, D., "Recent Developments in U.S. Engine Noise Reduction Research," NASA/TM—2001-211083, ISABE–2001–1017, 2001.
4. Podboy, G., Krupar, M., Helland, S., and Hughes, C., "Measurements of the Flow Within a NASA 22 Inch Fan Model," AIAA–2002–1033.
5. Yuska, J.A., Diedrich, J.H., and Nestor, C., "Lewis 9- by- 15-Foot V/STOL Wind Tunnel," NASA TM X–2305, 1971.
6. Arrington, A.E., and Gonsalez, J.C., "Flow Quality Improvements in the NASA Lewis Research Center 9- by 15-Foot Low Speed Wind Tunnel," NASA CR–195439, 1995.
7. Dahl, M.D. and Woodward, R.P., "Acoustical Evaluation of the NASA Lewis 9- By 15-Foot Low Speed Wind Tunnel," NASA TP–3274, 1992.
8. Balan, C. and Hoff, G.E., "Propulsion Simulator for High Bypass Turbofan Performance Evaluation," SAE 931410, 1993.

9. Envia, E. and Nallasamy, M., "Design Selection and Analysis of a Swept and Leaned Stator Concept," NASA/TM—1998-208662, 1998, Journal of Sound and Vibration, vol. 228, pp. 793–836, 1999.

10. Woodward, R.P., Elliot, D.M., Hughes, C.E., and Berton, J.J., "Benefits of Swept and Leaned Stators for Fan Noise Reduction," NASA/TM—1998-208661, AIAA–99–0479, AIAA Journal of Aircraft, vol. 38, no. 6, 2001.

Table 1. Fan design parameters

No. of Fan Blades	22
Fan Tip Diameter	22 in
Radius Ratio	0.30
Corrected Tip Speed	1,215 ft/sec
Corrected RPM	12,657
Corrected Fan Weight Flow	100.5 lbm/sec
Specific Flow	41.8 lbm/sec-ft^2
Stage Pressure Ratio	1.47
Design Bypass Ratio	8.85

Table 2. Summary of fan and OGV airfoil geometries

	Span	Fan	Baseline	Low Count	Low Noise
No. Blades/Vanes		22	54	26	26
Aft Sweep, deg		---	0	0	30
Aspect Ratio	Pitchline	2.00	3.51	1.67	1.67
Chord, in	Pitchline	3.61	1.57	3.26	3.26
Solidity	Hub		2.25	2.40	2.47
	Pitchline	1.73	1.52	1.51	1.53
	Tip		1.23	1.20	1.22
Stagger [1,2], deg	Hub		12.56	14.85	13.36
	Pitchline	37.10	10.29	10.68	10.75
	Tip		10.65	10.58	11.68
Vane Camber, deg	Hub	---	38.40	44.20	45.47
	Pitchline	---	34.56	37.57	36.06
	Tip	---	40.49	43.00	39.16
t_{max}/c	Hub	0.081	0.0707	0.0707	0.0638
	Pitchline	0.040	0.0702	0.0702	0.0640
	Tip	0.028	0.0698	0.0698	0.0639

[1]Defined from axial plane; positive angle in direction of fan rotation.
[2]Positive angle in opposite direction of fan rotation for OGVs.

Table 3. Summary of fan performance

Test Condition	Corrected Weight Flow, lbm/sec	Total Pressure Ratio	Total Temperature Ratio	Adiabatic Efficiency
Approach (61.7% NP_c)	58.3	1.159	1.049	0.889
Cutback (87.5% NP_c)	83.5	1.359	1.102	0.900
Takeoff (100% NP_c)	96.7	1.508	1.137	0.912
Design Point (100% NP_c)	100.5	1.488	1.130	0.924

Table 4. Summary of Baseline OGV performance

Test Condition	Corrected Weight Flow, lbm/sec	Total Pressure Ratio	Adiabatic Efficiency
Approach (61.7% NP_c)	58.5	1.154	0.860
Cutback (87.5% NP_c)	83.8	1.347	0.870
Takeoff (100% NP_c)	97.0	1.490	0.883
Design Point (100% NP_c)	100.5	1.470	0.890

Table 5. Summary of Low Count OGV performance

Test Condition	Corrected Weight Flow, lbm/sec	Total Pressure Ratio	Adiabatic Efficiency
Approach (61.7% NP_c)	58.5	1.154	0.861
Cutback (87.5% NP_c)	84.0	1.347	0.871
Takeoff (100% NP_c)	97.3	1.486	0.879
Design Point (100% NP_c)	100.5	1.470	0.891

Table 6. Summary of Low Noise OGV performance

Test Condition	Corrected Weight Flow, lbm/sec	Total Pressure Ratio	Adiabatic Efficiency
Approach (61.7% NP_c)	58.3	1.153	0.857
Cutback (87.5% NP_c)	83.5	1.343	0.865
Takeoff (100% NP_c)	96.7	1.483	0.872
Design Point (100% NP_c)	100.5	1.466	0.887

Table 7. Summary of stage losses for Baseline OGVs

OGV Configuration	Total Pressure Loss Coefficient, %	Adiabatic Efficiency Loss, %
Approach	0.46	2.83
Cutback	0.97	3.00
Takeoff	1.25	2.98
Design Point	1.33	3.29

Table 8. Summary of stage losses for Low Count OGVs

OGV Configuration	Total Pressure Loss Coefficient, %	Adiabatic Efficiency Loss, %
Approach	0.46	2.85
Cutback	1.00	3.06
Takeoff	1.43	3.38
Design Point	1.29	3.19

Table 9. Summary of stage losses for Low Noise OGVs

OGV Configuration	Total Pressure Loss Coefficient, %	Adiabatic Efficiency Loss, %
Approach	0.53	3.25
Cutback	1.16	3.58
Takeoff	1.66	3.94
Design Point	1.48	3.68

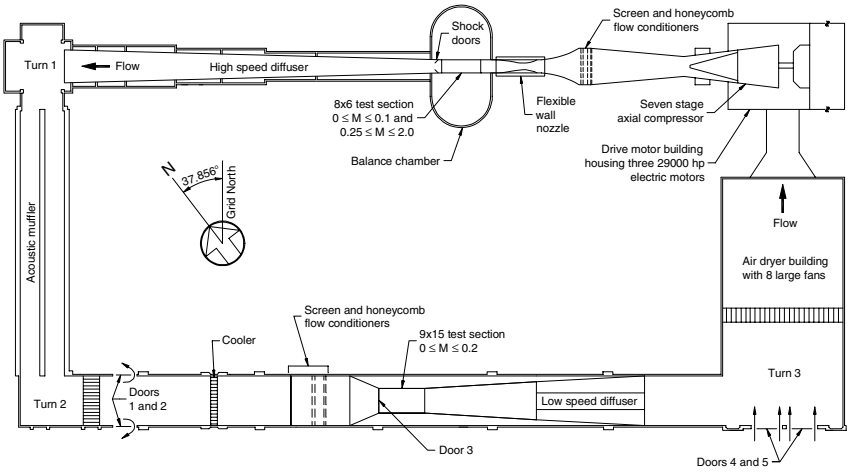

Figure 1. NASA Glenn Research Center 8- by 6-Foot Supersonic Wind Tunnel/9- by 15-Foot Low Speed Wind Tunnel Complex.

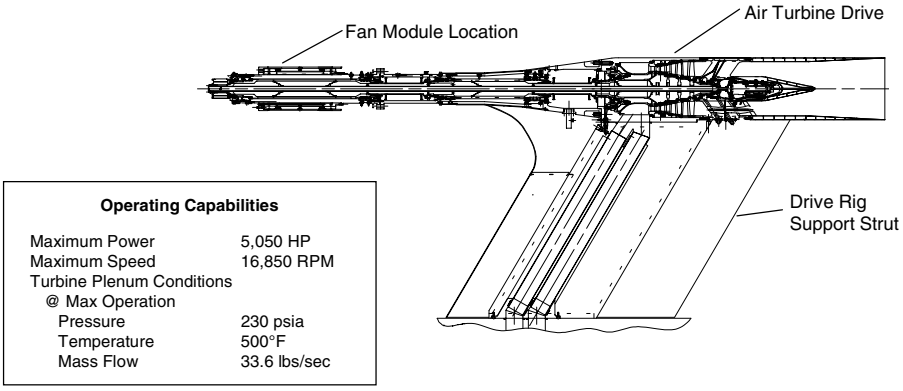

Figure 2. NASA Glenn Research Center Ultra High Bypass (UHB) Drive Rig propulsion simulator.

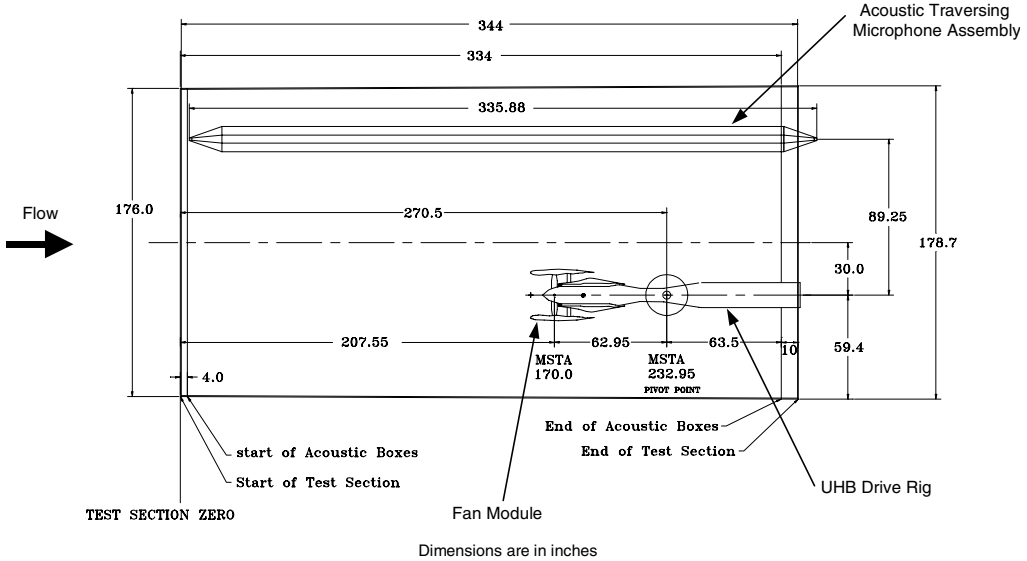

Figure 3. Top view schematic showing the location of the UHB Drive Rig in the 9- by 15-Foot Low Speed Wind Tunnel.

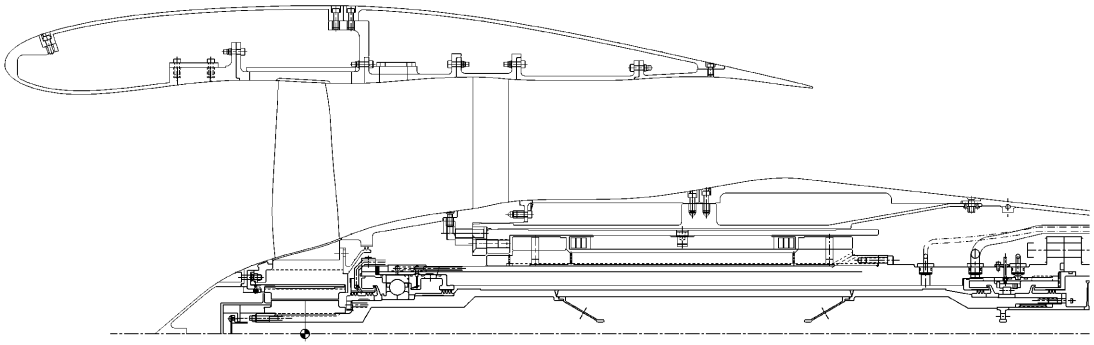

Figure 4. Schematic of the fan module in the acoustic testing configuration installed on the UHB Drive Rig.

Figure 5. Fan module in the acoustic testing configuration installed on the UHB Drive Rig in the NASA Glenn 9- by 15-Foot Low Speed Wind Tunnel.

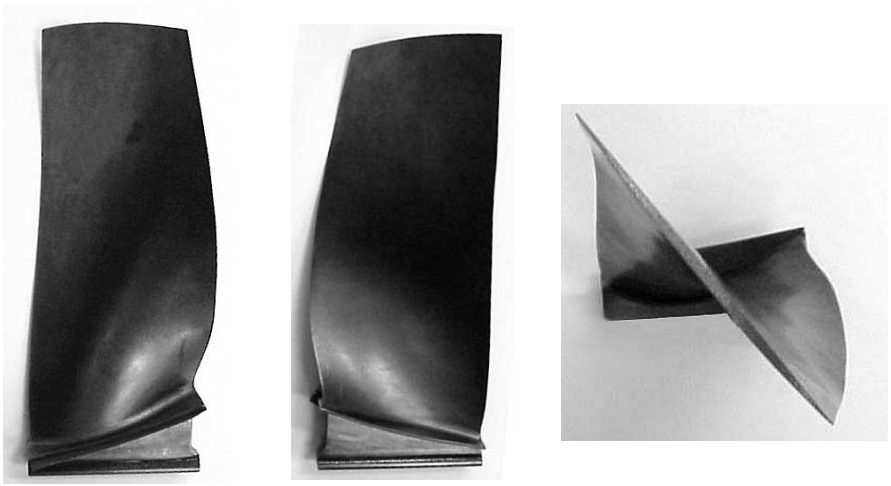

a. Suction surface b. Pressure surface c. Looking inboard from fan tip

Figure 6. Views of the fan blade.

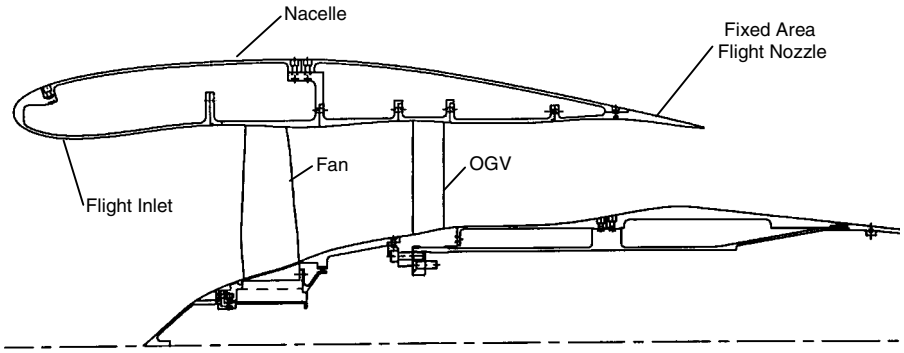

a. Schematic of fan module and Baseline OGV configuration.

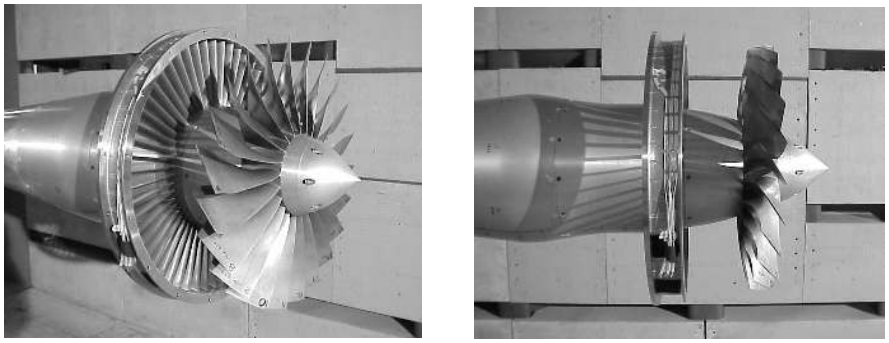

b. Fan and Baseline OGVs installed on the UHB Drive Rig in the 9x15.

Figure 7. Views of the Baseline OGV configuration.

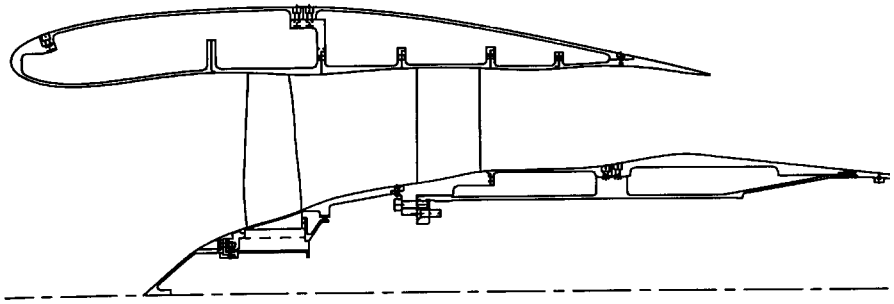

a. Schematic of fan module and Low Count OGV configuration.

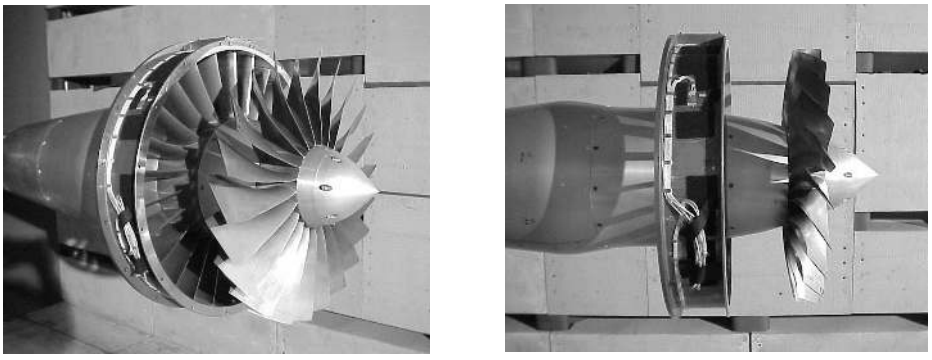

b. Fan and Low Count OGVs installed on the UHB Drive Rig in the 9x15.

Figure 8. Views of the Low Count OGV configuration.

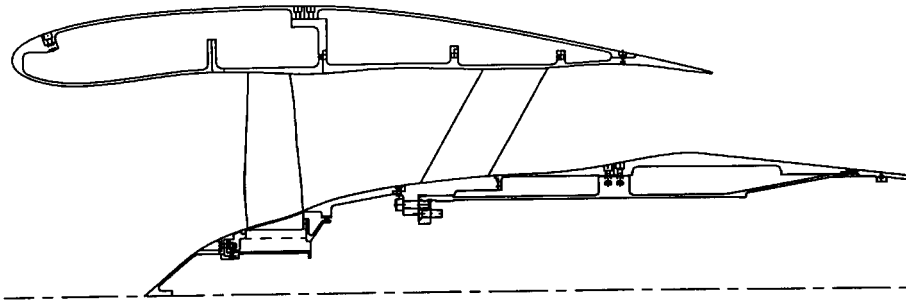

a. Schematic of the fan module and Low Noise OGV configuration.

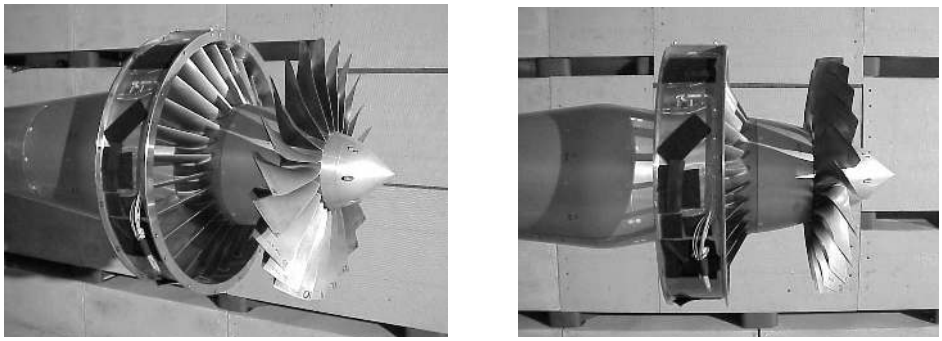

b. Fan and Low Noise OGVs installed on the UHB Drive Rig in the 9x15.

Figure 9. Views of the Low Noise OGV configuration.

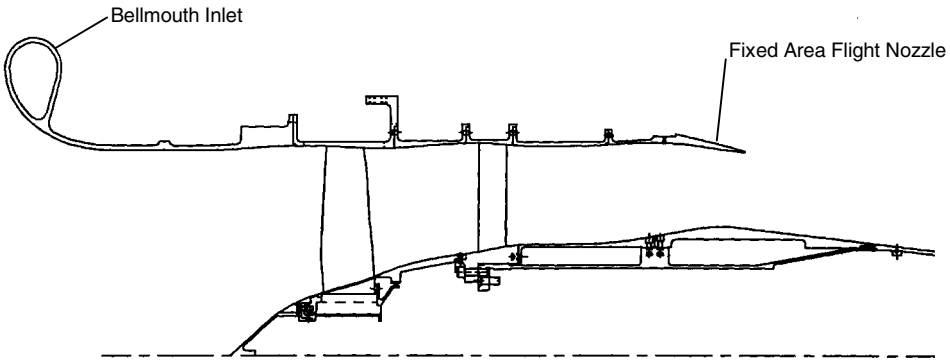

a. Schematic of the fan module in the fixed nozzle operating line performance testing configuration.

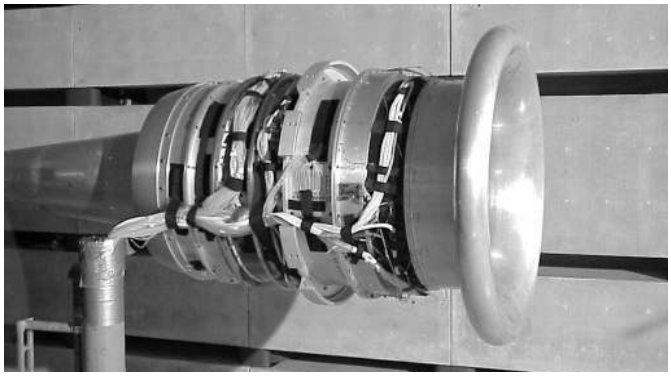

b. Fixed nozzle operating line performance testing configuration on the UHB Drive Rig in the 9x15.

Figure 10. Fan module in the fixed nozzle operating line performance testing configuration, with the bellmouth inlet and fixed area nozzle installed.

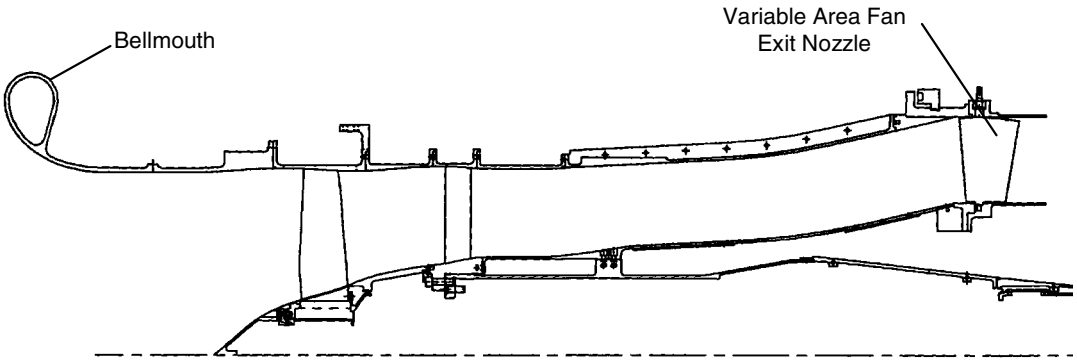

a. Schematic of the fan module in the mapping test configuration with the bellmouth inlet and VFEN.

b. Mapping testing configuration on the UHB Drive Rig in the 9x15.

c. Close-up view of the VFEN installation on the UHB Drive Rig.

Figure 11. Fan module in the fan and stage mapping performance testing configuration with bellmouth inlet and VFEN installed.

Figure 12. Fan module and freestream cruciform rake in the 9x15 during performance testing.

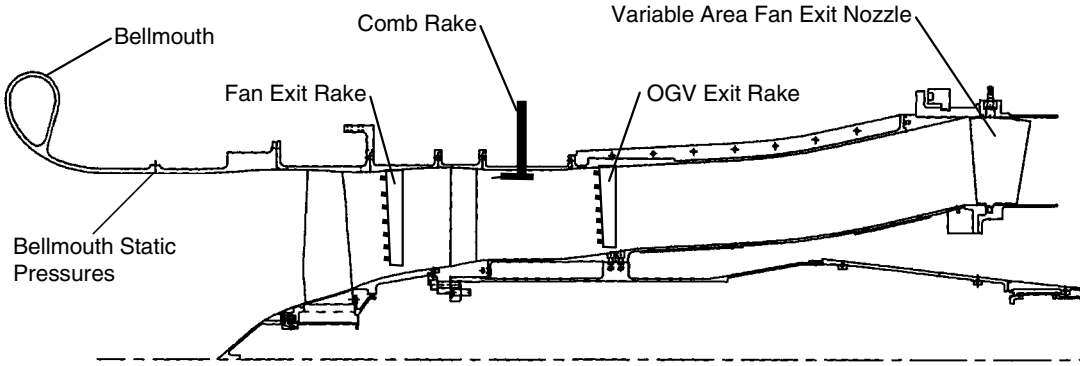

a. Mapping testing configuration.

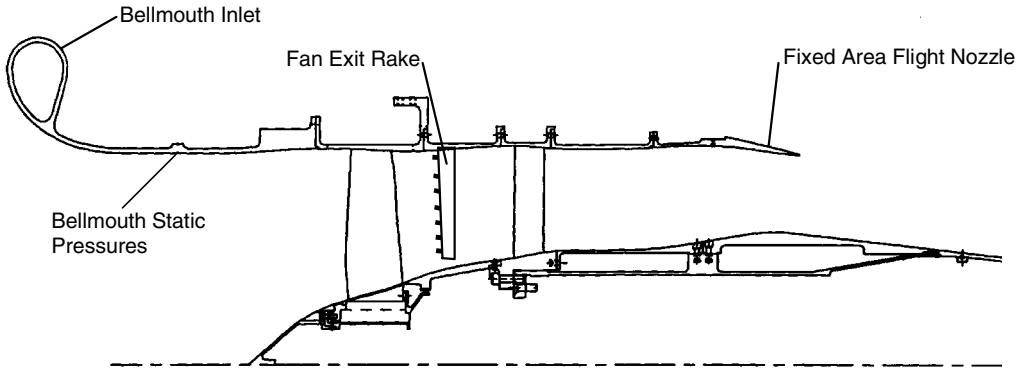

b. Fixed nozzle operating line testing configuration.

Figure 13. Schematic views of the instrumentation locations in the fan module during performance testing.

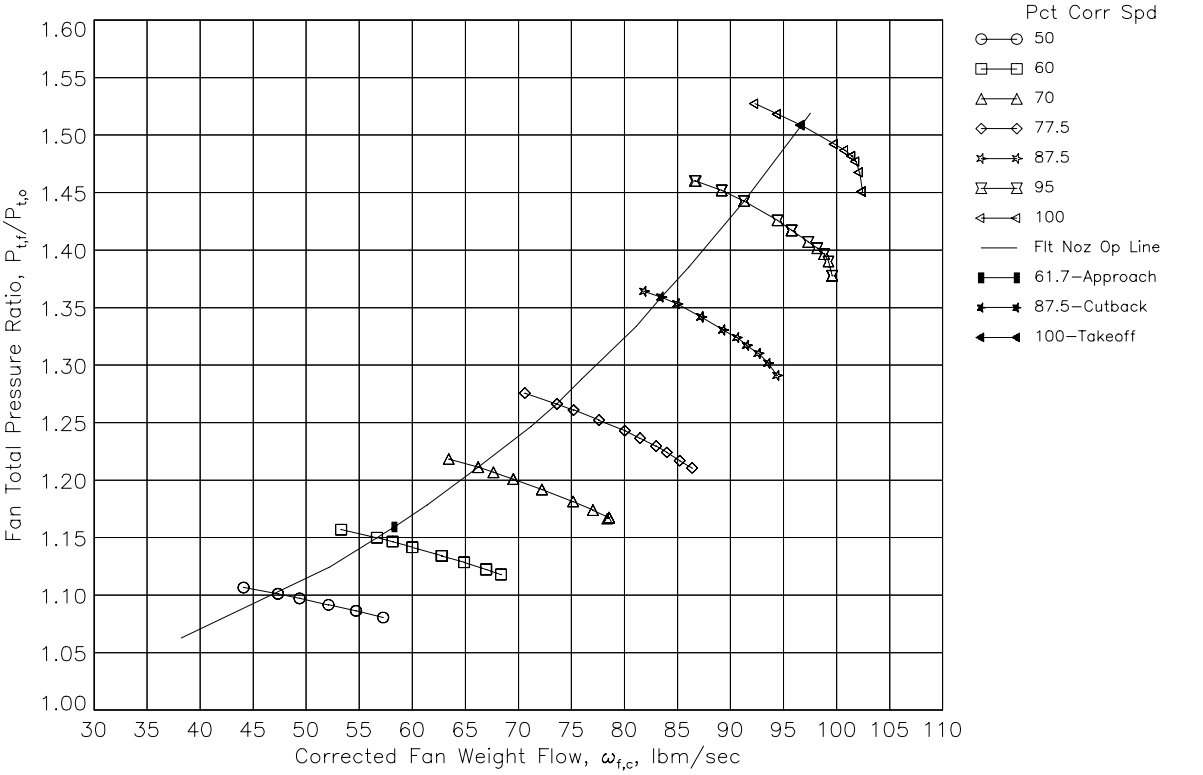

a. Total pressure ratio.

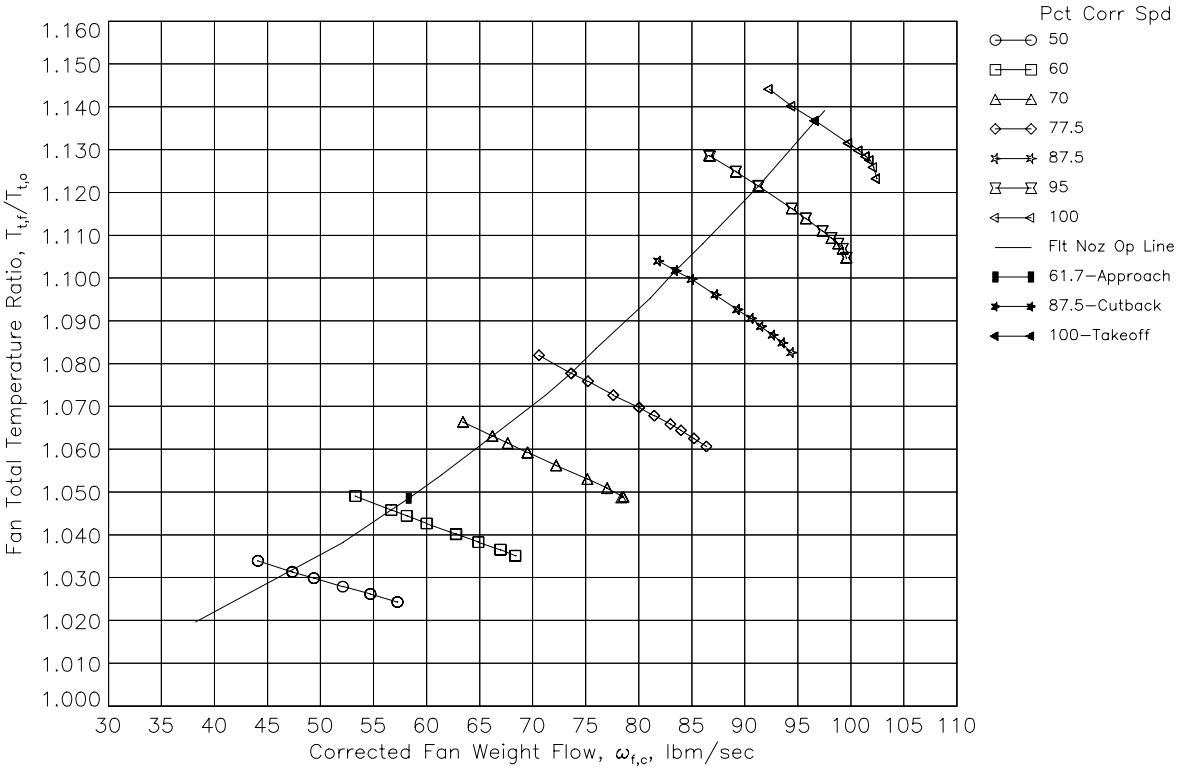

b. Total temperature ratio.

Figure 14. Fan performance maps with the Low Noise OGVs installed (continued).

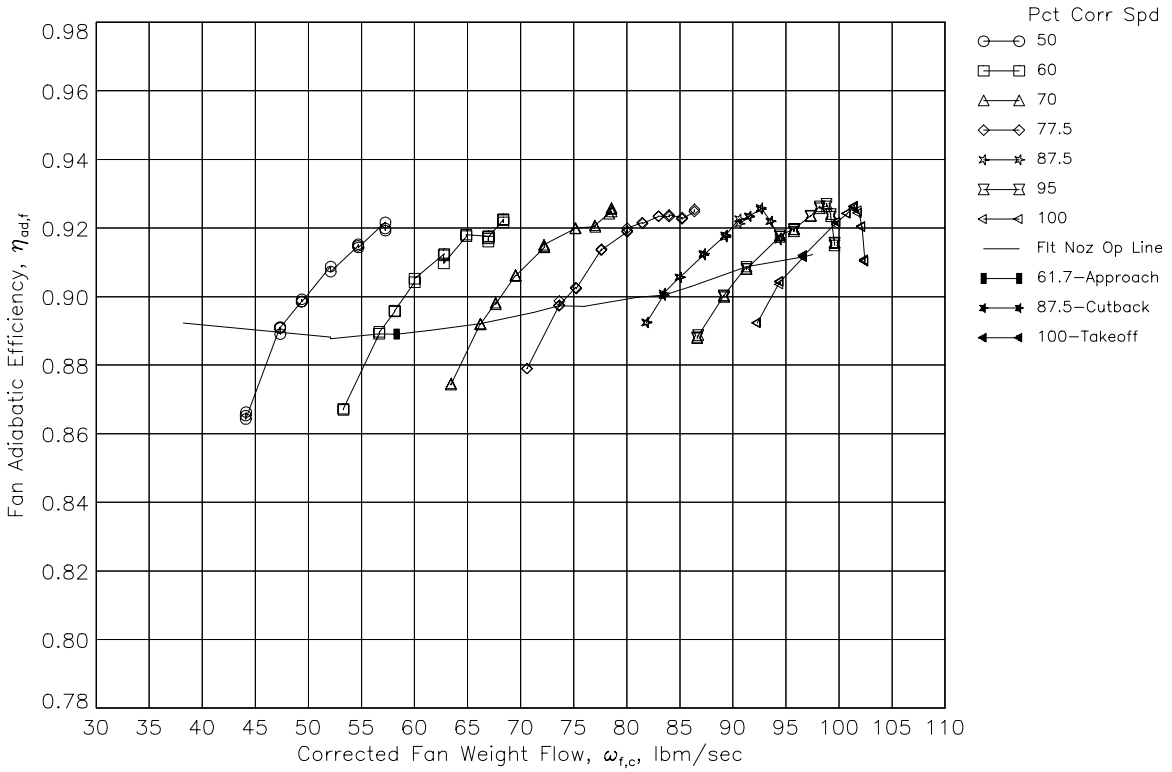

c. Adiabatic efficiency.

Figure 14. Fan performance map with the Low Noise OGVs installed (concluded).

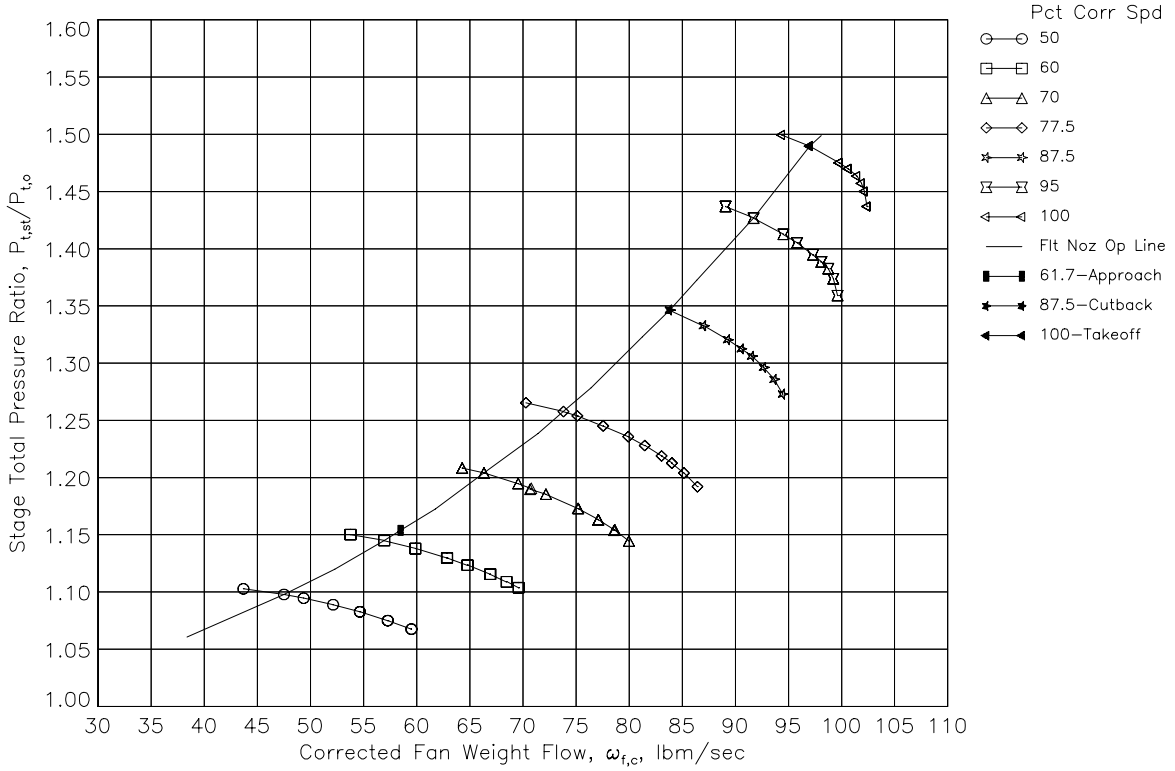

a. Total pressure ratio.

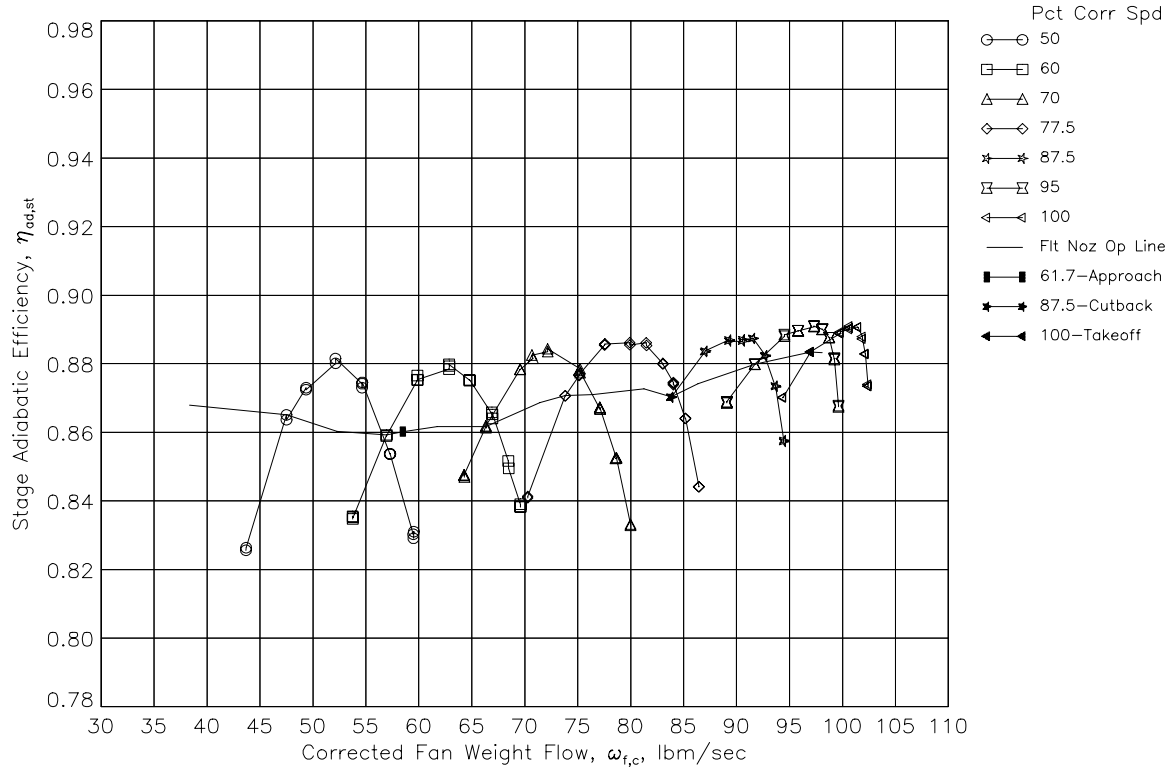

b. Adiabatic efficiency.

Figure 15. Stage performance map for the Baseline OGVs.

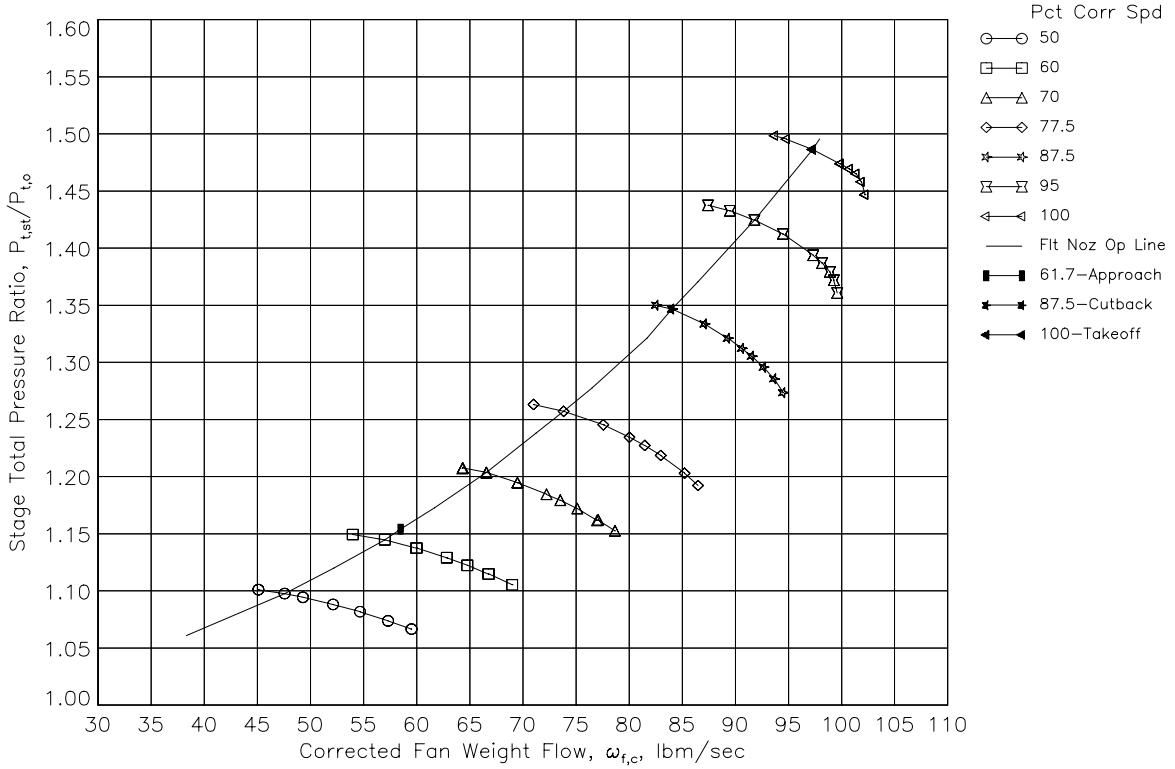

a. Total pressure ratio.

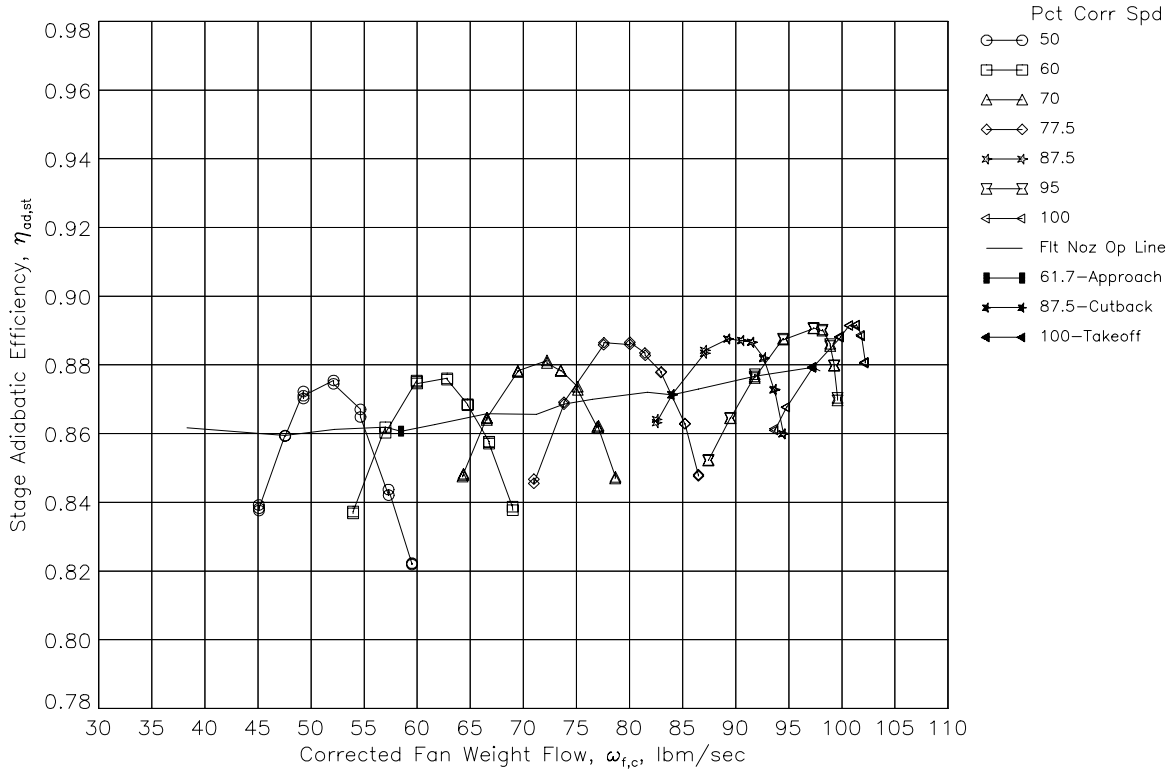

b. Adiabatic efficiency.

Figure 16. Stage performance map for Low Count OGVs.

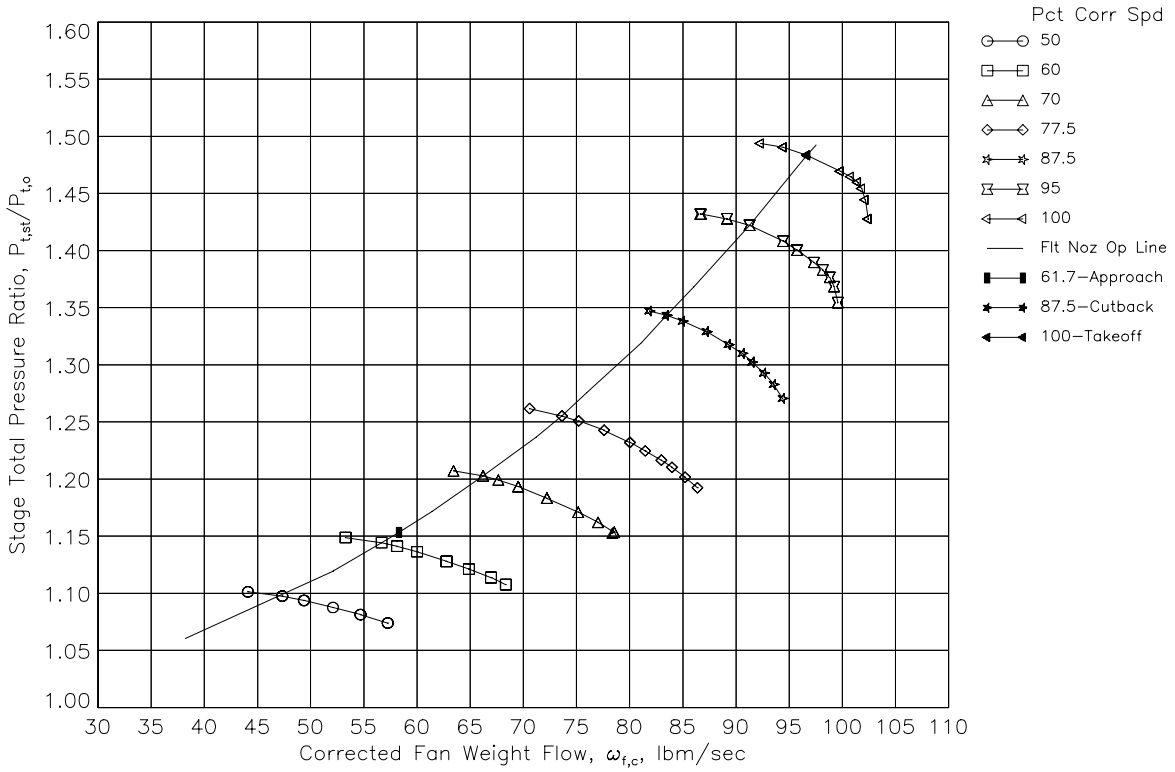

a. Total pressure ratio.

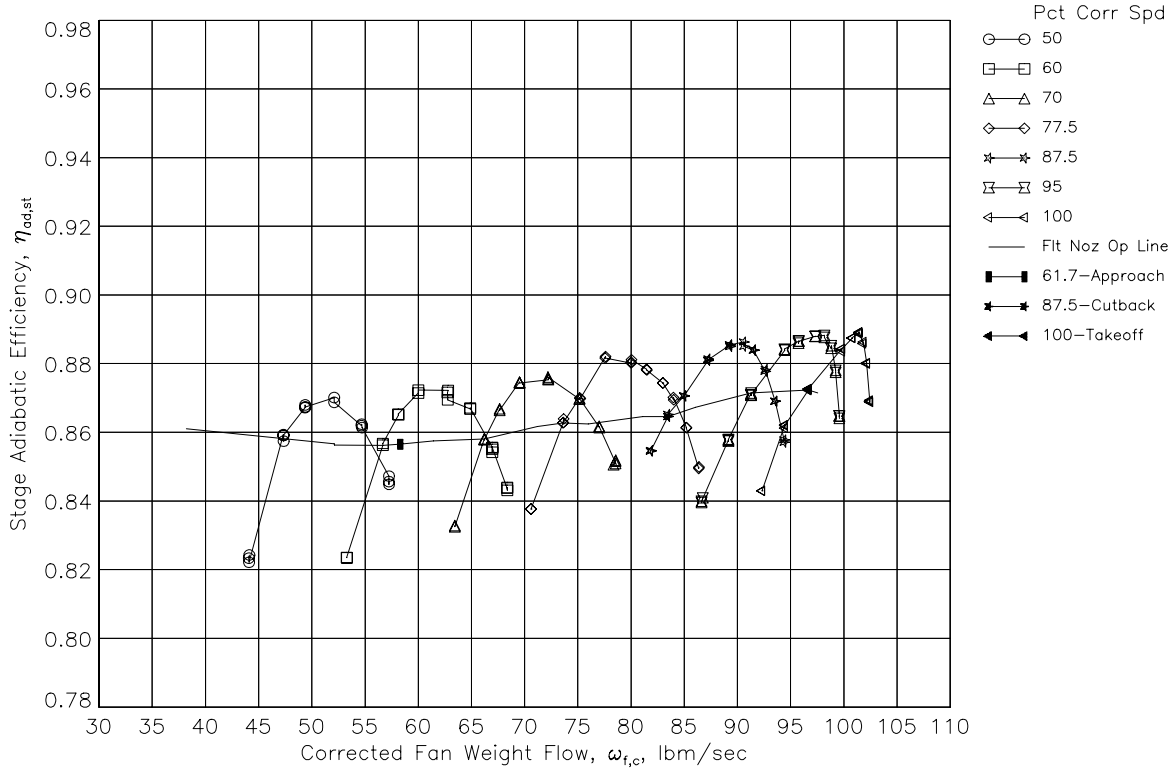

b. Adiabatic efficiency.

Figure 17. Stage performance map for Low Noise OGVs.

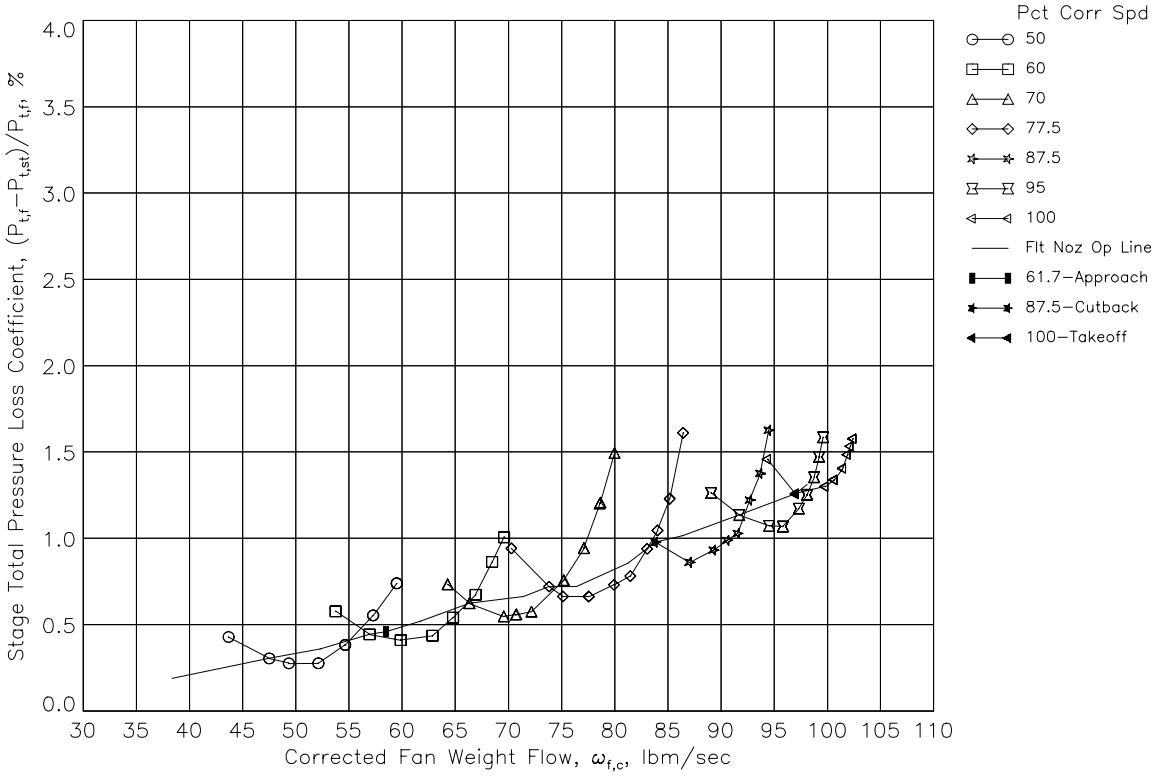

a. Total pressure loss coefficient.

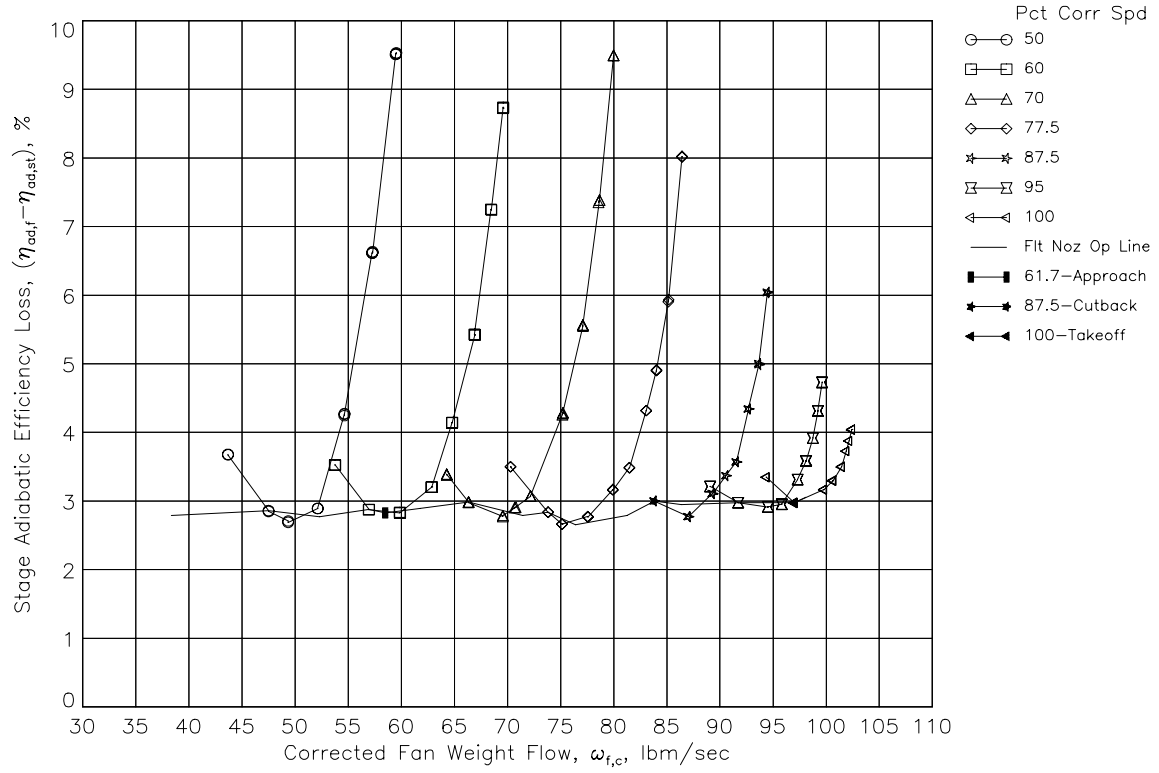

b. Adiabatic efficiency loss.

Figure 18. Stage performance loss coefficients for the Baseline OGVs.

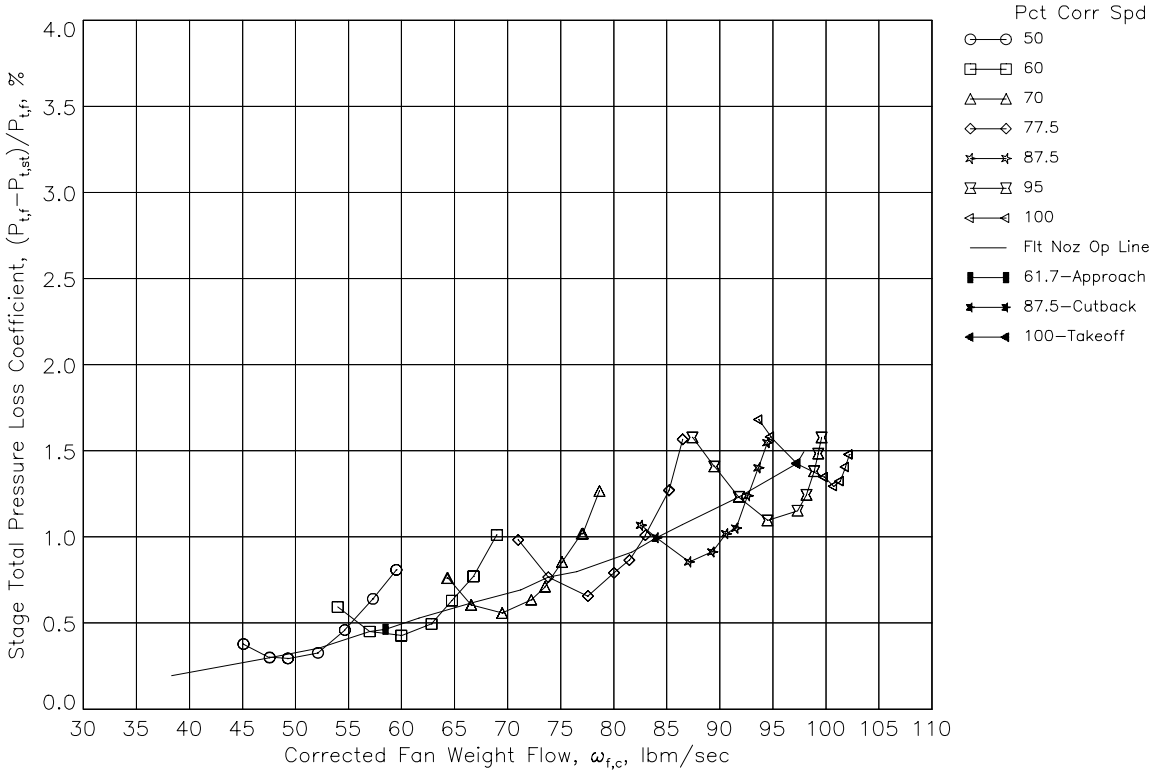

a. Total pressure loss coefficient.

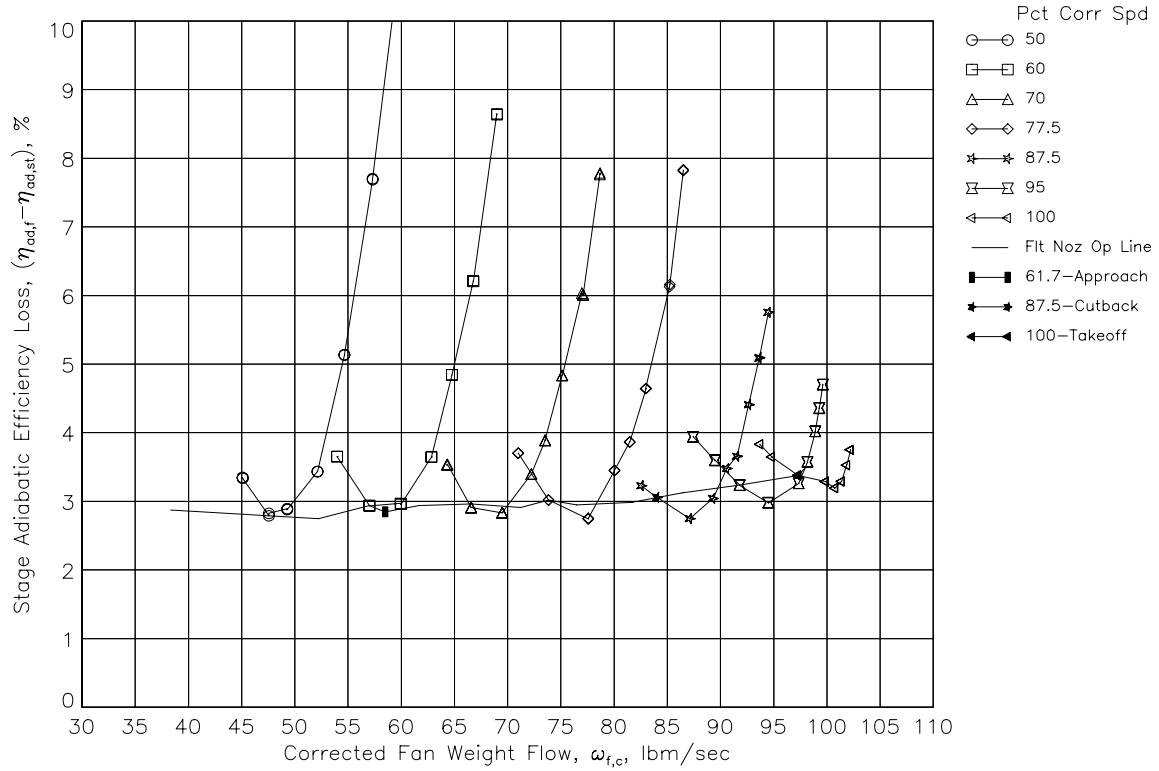

b. Adiabatic efficiency loss.

Figure 19. Stage performance loss coefficients for the Low Count OGVs.

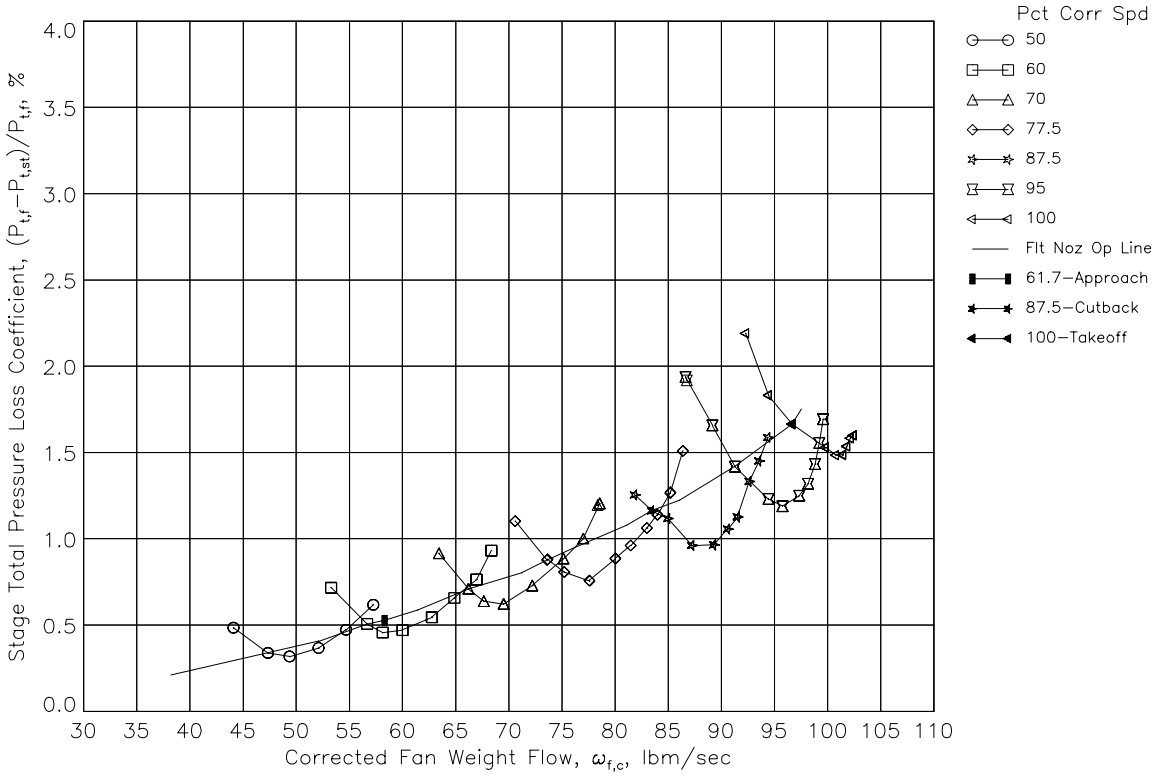

a. Total pressure loss coefficient.

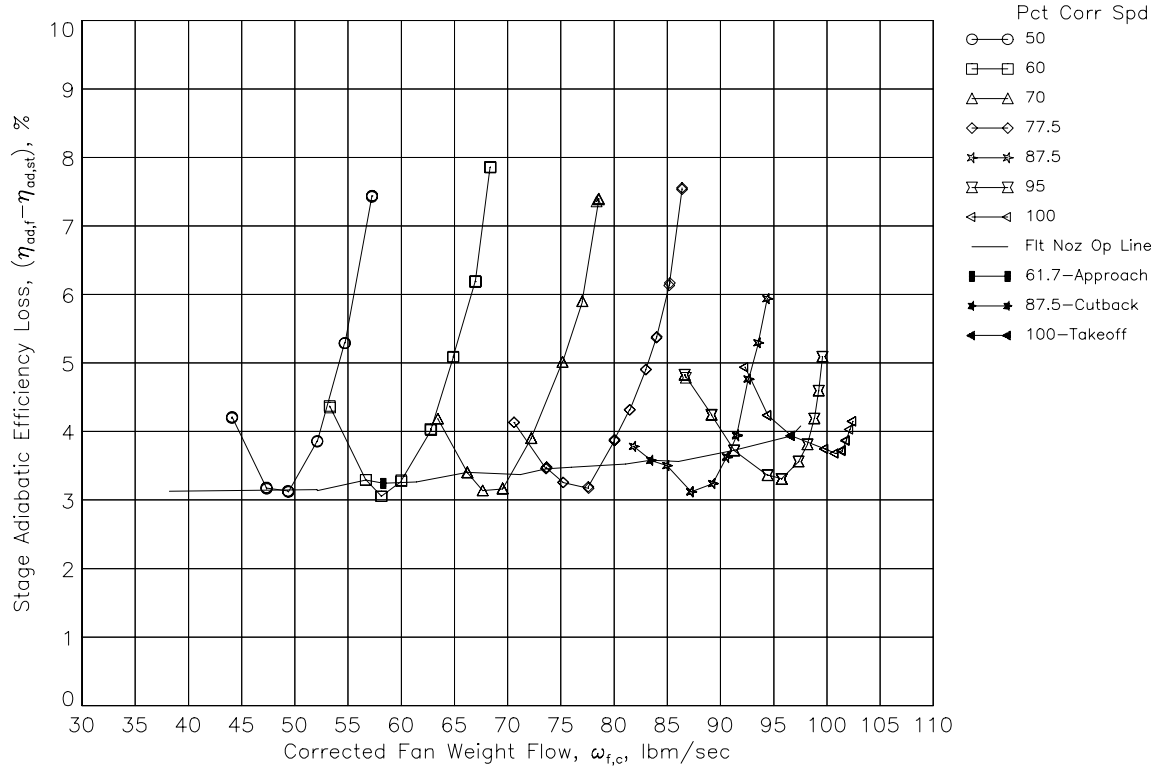

b. Adiabatic efficiency loss.

Figure 20. Stage performance loss coefficients for the Low Noise OGVs.

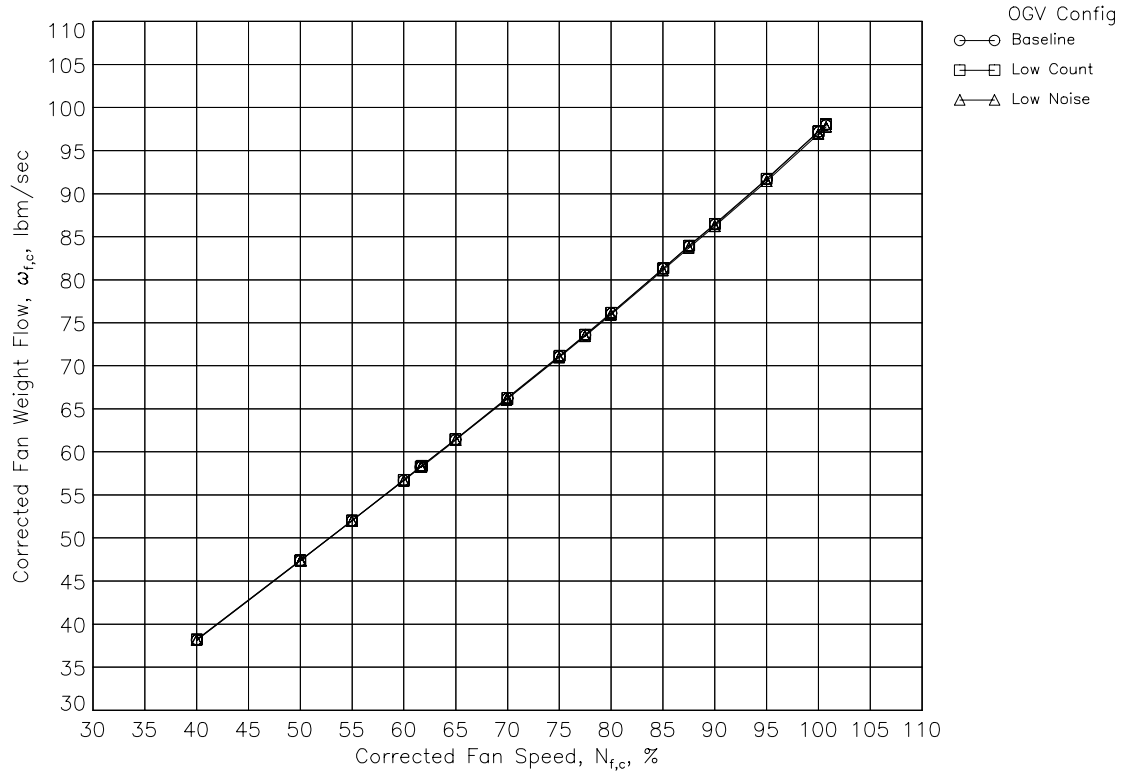

a. Corrected fan weight flow.

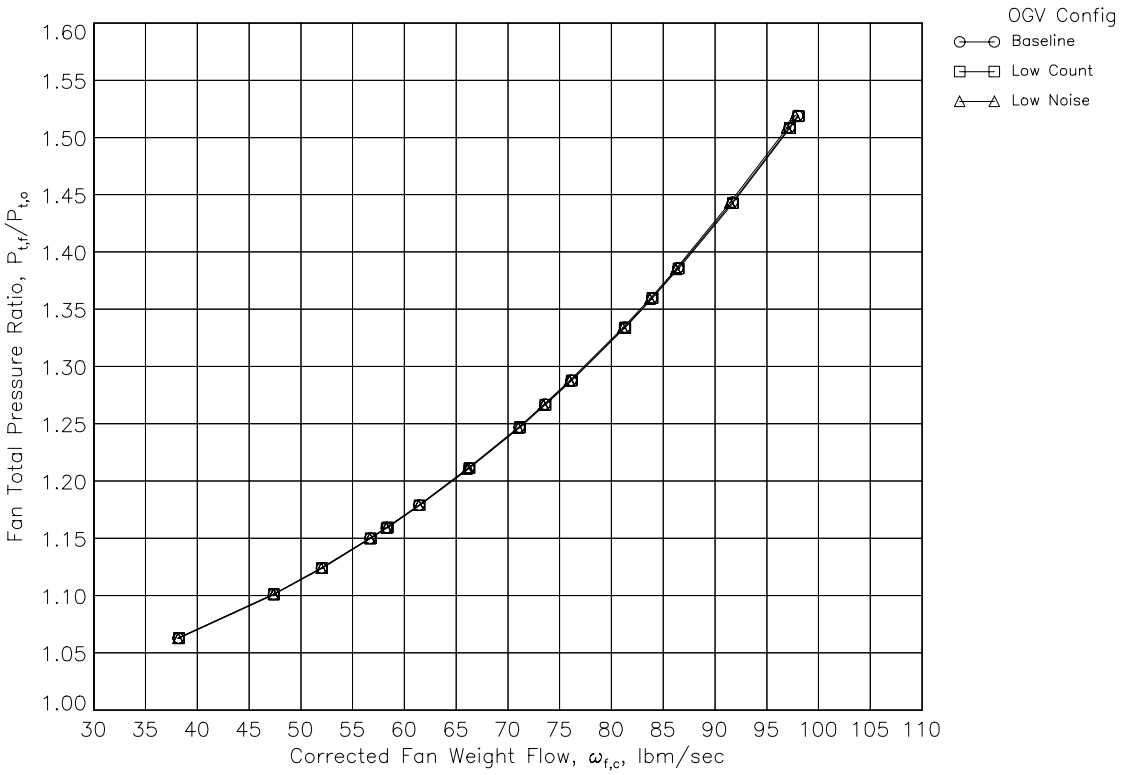

b. Total pressure ratio.

Figure 21. Fan performance comparison with OGV configuration on fixed area nozzle operating line (continued).

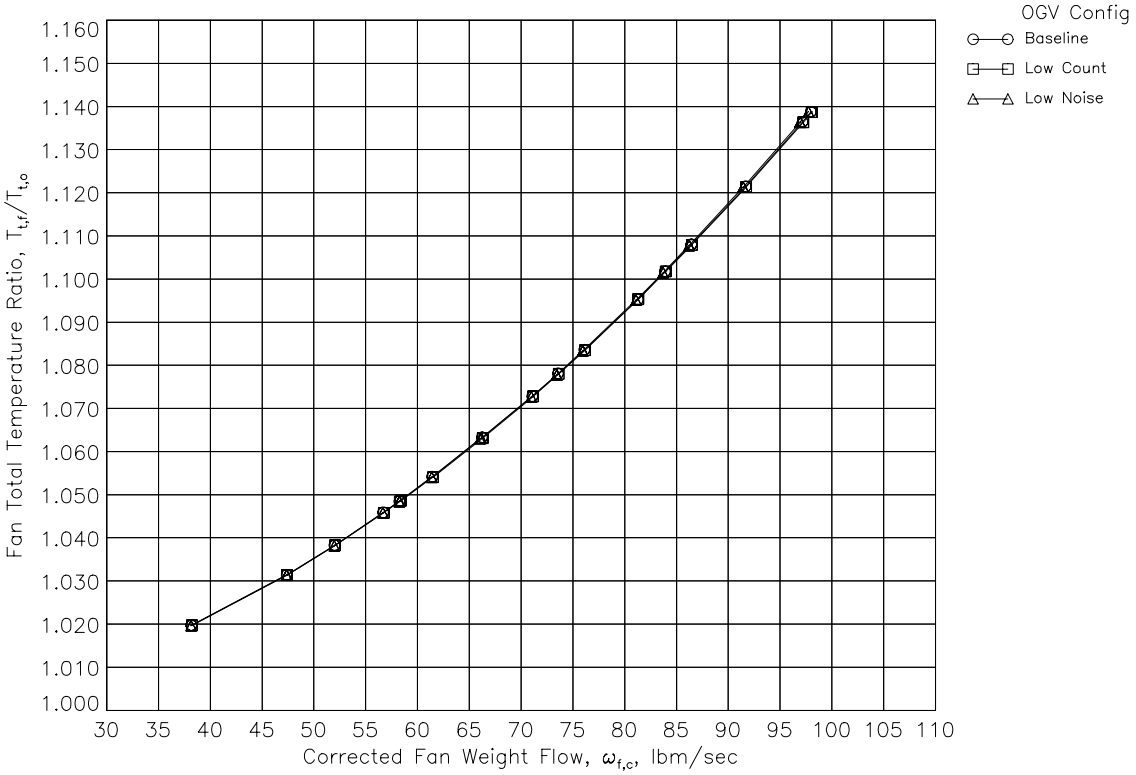

c. Total temperature ratio.

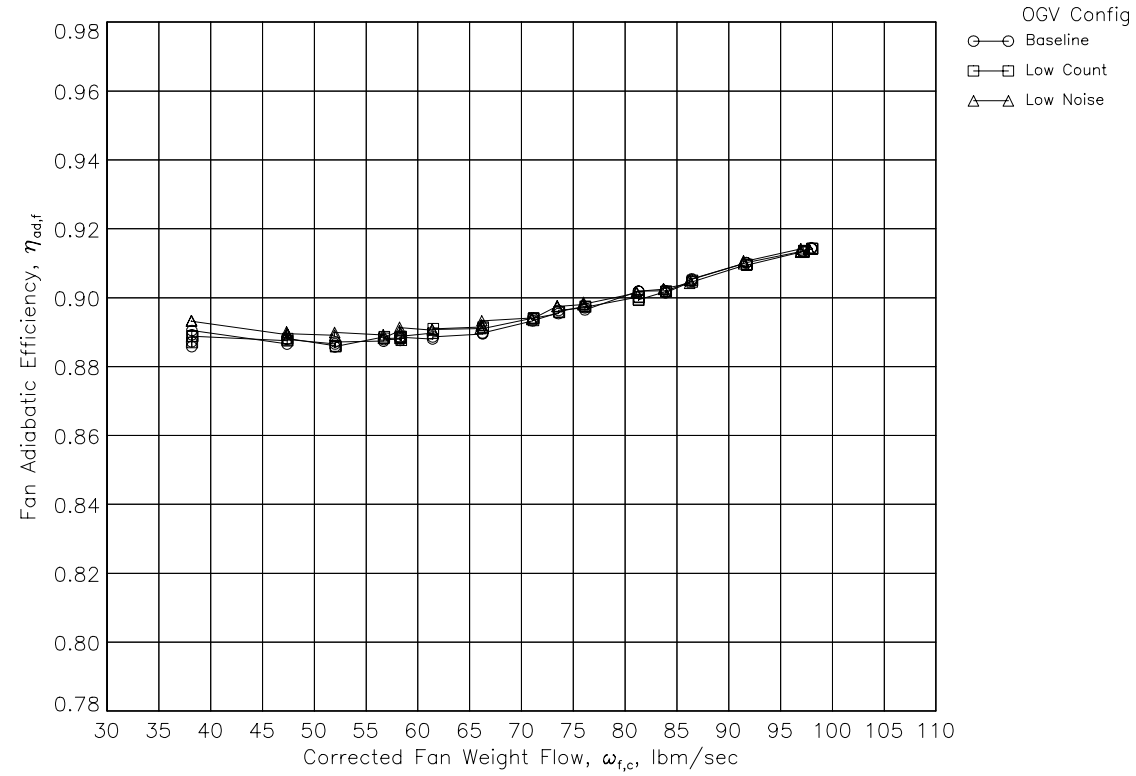

d. Adiabatic efficiency.

Figure 21. Fan performance comparison with OGV configuration on fixed area nozzle operating line (concluded).

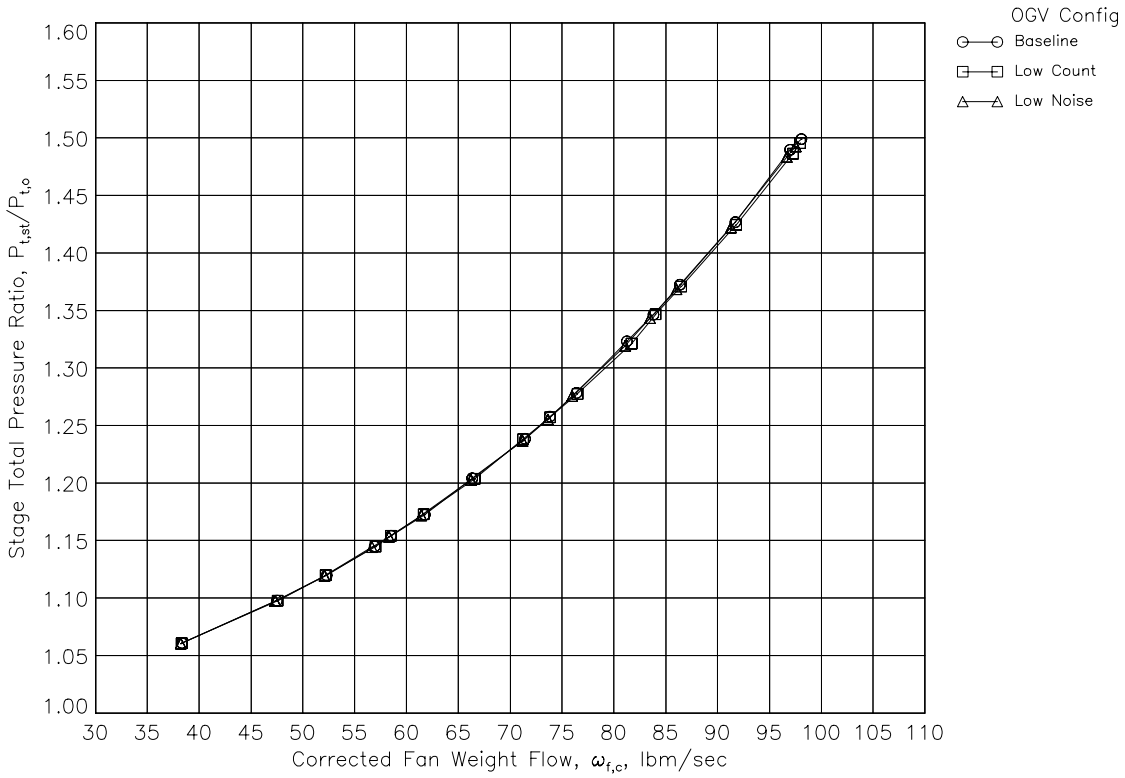

a. Total pressure ratio.

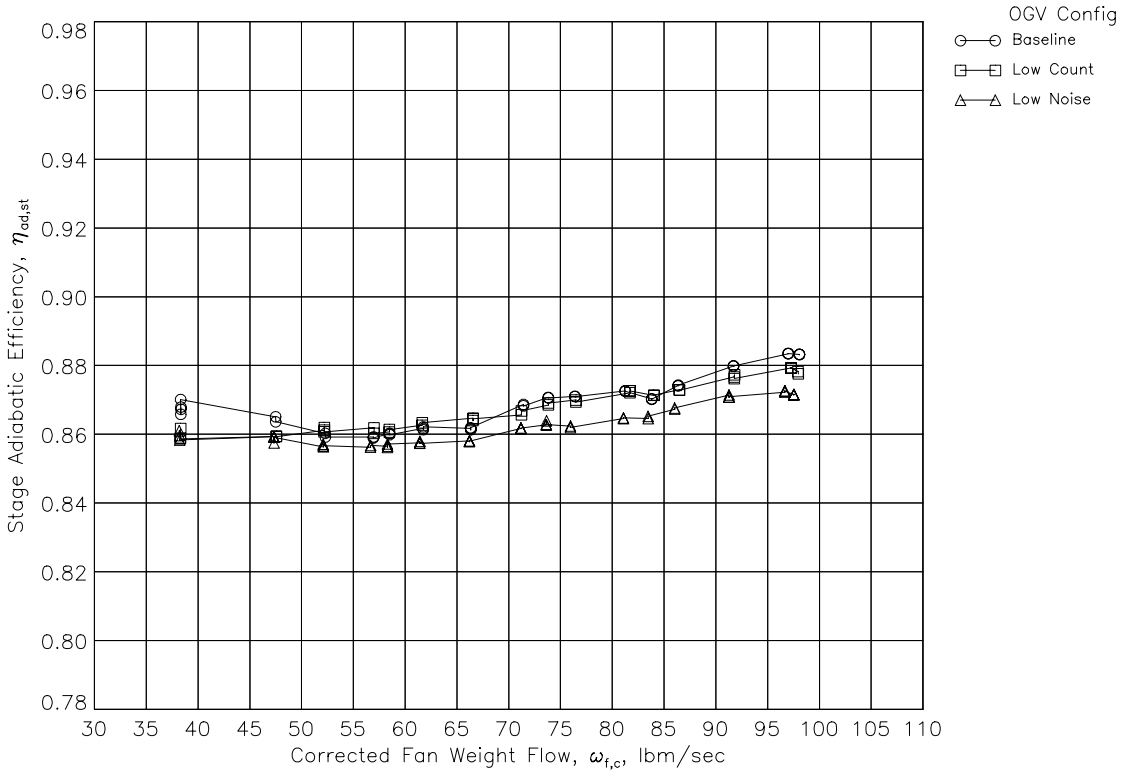

b. Adiabatic efficiency.

Figure 22. Stage performance comparison on the fixed area nozzle operating line.

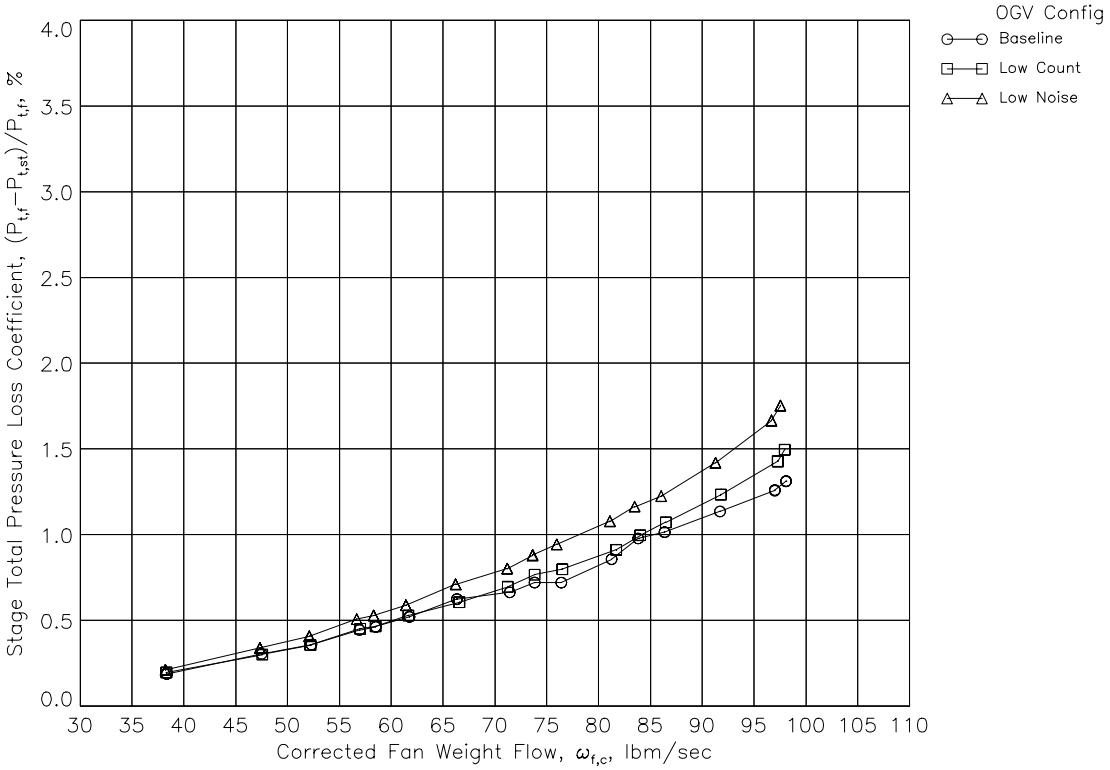

a. Total pressure coefficient loss.

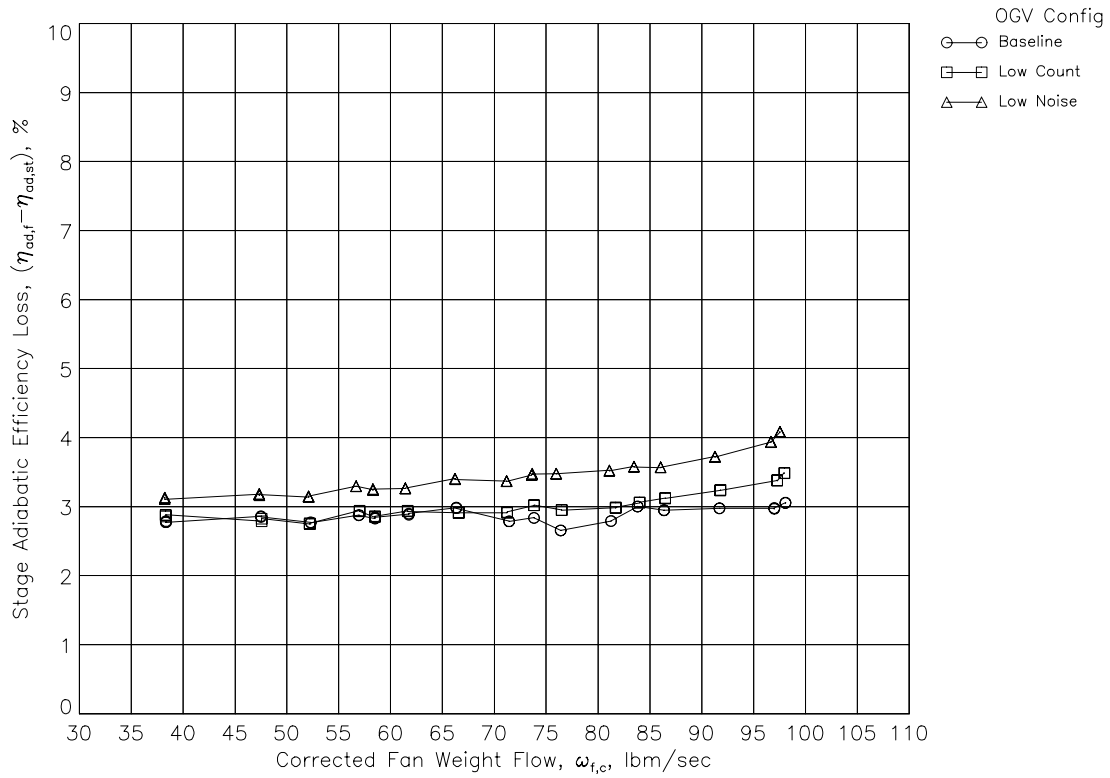

b. Adiabatic efficiency loss.

Figure 23. Stage performance loss comparison on the fixed area nozzle operating line.

REPORT DOCUMENTATION PAGE

Form Approved
OMB No. 0704-0188

1. AGENCY USE ONLY (*Leave blank*)	2. REPORT DATE	3. REPORT TYPE AND DATES COVERED
	December 2001	Technical Memorandum

4. TITLE AND SUBTITLE

Aerodynamic Performance of Scale-Model Turbofan Outlet Guide Vanes Designed for Low Noise

5. FUNDING NUMBERS

WU–781–30–11

6. AUTHOR(S)

Christopher E. Hughes

7. PERFORMING ORGANIZATION NAME(S) AND ADDRESS(ES)

National Aeronautics and Space Administration
John H. Glenn Research Center at Lewis Field
Cleveland, Ohio 44135–3191

8. PERFORMING ORGANIZATION REPORT NUMBER

E–13168

9. SPONSORING/MONITORING AGENCY NAME(S) AND ADDRESS(ES)

National Aeronautics and Space Administration
Washington, DC 20546–0001

10. SPONSORING/MONITORING AGENCY REPORT NUMBER

NASA TM—2001-211352
AIAA–2002–0374

11. SUPPLEMENTARY NOTES

Prepared for the 40th Aerospace Sciences Meeting and Exhibit sponsored by the American Institute of Aeronautics and Astronautics, Reno, Nevada, January 14–17, 2002. Responsible person, Christopher E. Hughes, organization code 5940, 216–433–3924.

12a. DISTRIBUTION/AVAILABILITY STATEMENT

Unclassified - Unlimited
Subject Category: 02 Distribution: Nonstandard

Available electronically at http://gltrs.grc.nasa.gov/GLTRS

This publication is available from the NASA Center for AeroSpace Information, 301–621–0390.

12b. DISTRIBUTION CODE

13. ABSTRACT ***(Maximum 200 words)***

The design of effective new technologies to reduce aircraft propulsion noise is dependent on an understanding of the noise sources and noise generation mechanisms in the modern turbofan engine. In order to more fully understand the physics of noise in a turbofan engine, a comprehensive aeroacoustic wind tunnel test program was conducted called the "Source Diagnostic Test." The test was cooperative effort between NASA and General Electric Aircraft Engines, as part of the NASA Advanced Subsonic Technology Noise Reduction Program. A 1/5-scale model simulator representing the bypass stage of a current technology high bypass ratio turbofan engine was used in the test. The test article consisted of the bypass fan and outlet guide vanes in a flight-type nacelle. The fan used was a medium pressure ratio design with 22 individual, wide chord blades. Three outlet guide vane design configurations were investigated, representing a 54-vane radial Baseline configuration, a 26-vane radial, wide chord Low Count configuration and a 26-vane, wide chord Low Noise configuration with 30° of aft sweep. The test was conducted in the NASA Glenn Research Center 9- by 15-Foot Low Speed Wind Tunnel at velocities simulating the takeoff and approach phases of the aircraft flight envelope. The Source Diagnostic Test had several acoustic and aerodynamic technical objectives: first, establish the performance of a scale model fan selected to represent the current technology turbofan product; second, assess the performance of the fan stage with each of the three distinct outlet guide vane designs; third, determine the effect of the outlet guide vane configuration on the fan baseline performance; and finally, conduct detailed flowfield diagnostic surveys, both acoustic and aerodynamic, to characterize and understand the noise generation mechanisms in a turbofan engine. This paper addresses the fan and stage aerodynamic performance results from the Source Diagnostic Test.

14. SUBJECT TERMS	15. NUMBER OF PAGES
Wind tunnel; Wind tunnel model; Powered model; Scale model; Turbofan; Fan; Vane; Ducted fan; Fan blade; Stator; Turbomachinery; Performance; Efficiency	39
	16. PRICE CODE

17. SECURITY CLASSIFICATION OF REPORT	18. SECURITY CLASSIFICATION OF THIS PAGE	19. SECURITY CLASSIFICATION OF ABSTRACT	20. LIMITATION OF ABSTRACT
Unclassified	Unclassified	Unclassified	